TÜBİTAK

Turkish Journal of Earth Sciences

http://journals.tubitak.gov.tr/earth/

Research Article

Turkish J Earth Sci
(2013) 22: 747-777

doi:10.3906/yer-1207-10

# Palaeoenvironmental and chronological constraints on the Tuğlu Formation (Çankırı Basin, Central Anatolia, Turkey)

**Ilaria MAZZINI[1],*,**, Natália HUDÁČKOVÁ[2], Peter JONIAK[2], Marianna KOVÁČOVÁ[2], Tamás MIKES[3,4], Andreas MULCH[3,4,5], F. Bora ROJAY[6], Stella LUCIFORA[7], Daniela ESU[1,8], Ingeborg SOULIÉ-MÄRSCHE[9]**

[1]IGAG-CNR, Rome, Italy

[2]Department of Geology and Palaeontology, Faculty of Natural Sciences, Comenius University in Bratislava, 842 15 Bratislava, Slovakia

[3]Biodiversity and Climate Research Centre, D-60325 Frankfurt am Main, Germany

[4]Goethe University, Institute of Geosciences, D-60438 Frankfurt am Main, Germany

[5]Senckenberg Research Institute and Natural History Museum, D-60325 Frankfurt am Main, Germany

[6]Department of Geological Engineering, Faculty of Engineering, Middle East Technical University, 06531 Ankara, Turkey

[7]Department of Earth Sciences, Roma Tre University, Rome, Italy

[8]Department of Earth Sciences, Sapienza University of Rome, 00185 Rome, Italy

[9]Institut des Sciences de l'Evolution, University Montpellier 2, 34095 Montpellier-Cedex 5, France

**Received:** 27.07.2012 • **Accepted:** 29.11.2012 • **Published Online:** 26.08.2013 • **Printed:** 25.08.2013

**Abstract:** The Çankırı Basin, located in the northern part of the Central Anatolian Plateau, is a large Tertiary basin where thick Miocene to Quaternary continental sediments overlay the Cretaceous-Tertiary units. This investigation focuses on the Tuğlu Formation, an Upper Miocene succession mainly composed of dark grey silty and organic rich clays. The type section of Tuğlu has been sampled for an array of multidisciplinary analyses. The palaeontological proxies included ostracod, foraminifer, nannoplankton, pollen, molluscs, charophytes, small mammal assemblages, fish, and crab remains. The abiotic parameters studied were: palaeomagnetism and environmental magnetism, stable carbon and oxygen isotope ratios (on ostracods and bulk sediment samples), strontium isotope ratios (on ostracods and foraminifera), and major elemental composition of the sediments. All analysed proxies point to a continental setting characterised by permanent water bodies affected by strong salinity oscillations. A shallow saline lake developed in a permanent freshwater lake. Barren layers, potentially linked to a short subaerial exposure, mark the end of the saline lake and the transition to a fluvial environment. Geochemical analysis confirms aridity–humidity oscillations as recorded by the micropalaeontological proxies. Analysis of small mammal assemblages refined the chronology of the Tuğlu Formation, with the onset of the deposition at the base of the mammal zone MN9 (around 11 Ma) and continuous deposition until the MN11 zone (around 8 Ma). The stable oxygen isotope records from the Tuğlu section point to Miocene $\delta^{18}O$ water values consistent with subdued topography where no prominent mountain belts were yet developed at the northern plateau margin. If correct, this suggests that at least until the end of the deposition of the Tuğlu Formation, the Çankırı Basin did not yet experience rain shadow conditions, and the regional surface uplift of the area most likely occurred after 8 Ma.

**Key words:** Late Miocene, palaeoenvironment, palaeoclimate, biostratigraphy, stable isotopes, palaeomagnetism

## 1. Introduction

The Çankırı Basin, located in the northern part of the Central Anatolian Plateau (CAP), is a large Tertiary basin with thick Miocene to Quaternary continental sediments overlying deformed Mesozoic to older Tertiary units. The Miocene continental successions have provided rich large and small mammal assemblages (Sen *et al.* 1998; Kaymakci 2000; Ünay *et al.* 2003), which allowed a precise biostratigraphic age assignment and yielded additional valuable palaeoenvironmental information. In particular, the Tuğlu Formation represents a key point to understand the evolution of the basin during the Late Miocene, when the uplift of the CAP margins started (Yildirim *et al.* 2011; Cosentino *et al.* 2012; Schildgen *et al.* 2012). Here we describe the type section of the Tuğlu Formation, a sequence exceptionally rich in fossils. The section has been sampled for micropalaeontological (ostracods, foraminifera, pollen, Characeae), palaeontological (molluscs, small mammals, fish remains), environmental magnetism, and stable carbon and oxygen isotope analyses (on ostracods and bulk sediment samples) as well as strontium isotope analyses (on ostracods and foraminifera) and major elements composition of the sediments. Through a highly multidisciplinary approach, we document the

* Correspondence: ilaria.mazzini@igag.cnr.it

** Current address: Department of Environmental Biology, Roma 3 University, Viale Marconi 466, Rome, Italy

palaeoenvironmental and palaeoclimatic evolution of the basin and discuss it in the context of the Late Neogene uplift history of the CAP.

## 2. Geologic overview

The Çankırı Basin is an important element in understanding the Miocene evolution of Central Anatolia. The basin formed on top of a Cretaceous-Palaeogene accretionary wedge and the so-called Kırşehir crystalline indenter (Figure 1A) following the final closure of the northern branch of the Neotethys during the Miocene (Gansser 1974; Şengör & Yılmaz 1981; Kaymakçı 2000; Rojay 2012). The closure ended with continental collision, with development of Miocene basins in Central Anatolia (e.g., Ankara and Çankırı basins) partially to completely isolated from the Mediterranean and Eastern Paratethys seaways, and with extensive Neogene volcanism (e.g., Galatian and Cappadocian volcanic provinces).

The Çankırı Basin is bounded by Cretaceous ophiolitic mélanges to the north and to the west, by sinistral leaky transform fault overprinting the imbricated accretionary wedge to the east, and by the Kırşehir crystalline complex to the south (Figure 1A). The Miocene Çankırı Basin can be differentiated into 2 sectors: the western part (Hancılı area) and the main central part (Çankırı Basin). In the central part, the infilling sediments were deposited during 3 different sedimentary cycles (Kaymakçı 2000; Kaymakçı *et al*., 2000, 2003): the first cycle is represented by fluvio-lacustrine clastic sediments of Early to Middle Miocene age (Kılçak and Çandır formations); the second cycle is made up of continental sediments alternating with evaporites of Middle to Late Miocene age (Tuğlu, Süleymanlı, and Bozkır formations); the third cycle includes Plio-Quaternary (Değim Formation) and recent alluvial to colluvial deposits.

Following the Late Paleocene to pre-Early Miocene compressional tectonic phase (phase 2 sensu Kaymakçı *et al.* 2003), the Lower Miocene basal red clastics and lacustrine mudrocks were deposited in an extensional setting. The Lower Miocene sediments were intensely folded and deformed prior to the Late Miocene. The deposition of the Middle to Upper Miocene deposits occurred in an extensional basin as manifested by ENE-WSW trending syn-sedimentary normal faults. The Upper Pliocene deposits (MN17, Değim Formation per partem, Kaymakçı 2000) unconformably overlie steeply tilted to overturned Miocene sequences that were thrusted by Cretaceous ophiolitic mélange. The counter-clockwise rotational westward escape of the Anatolian plate between the North Anatolian Fault in the north and the East

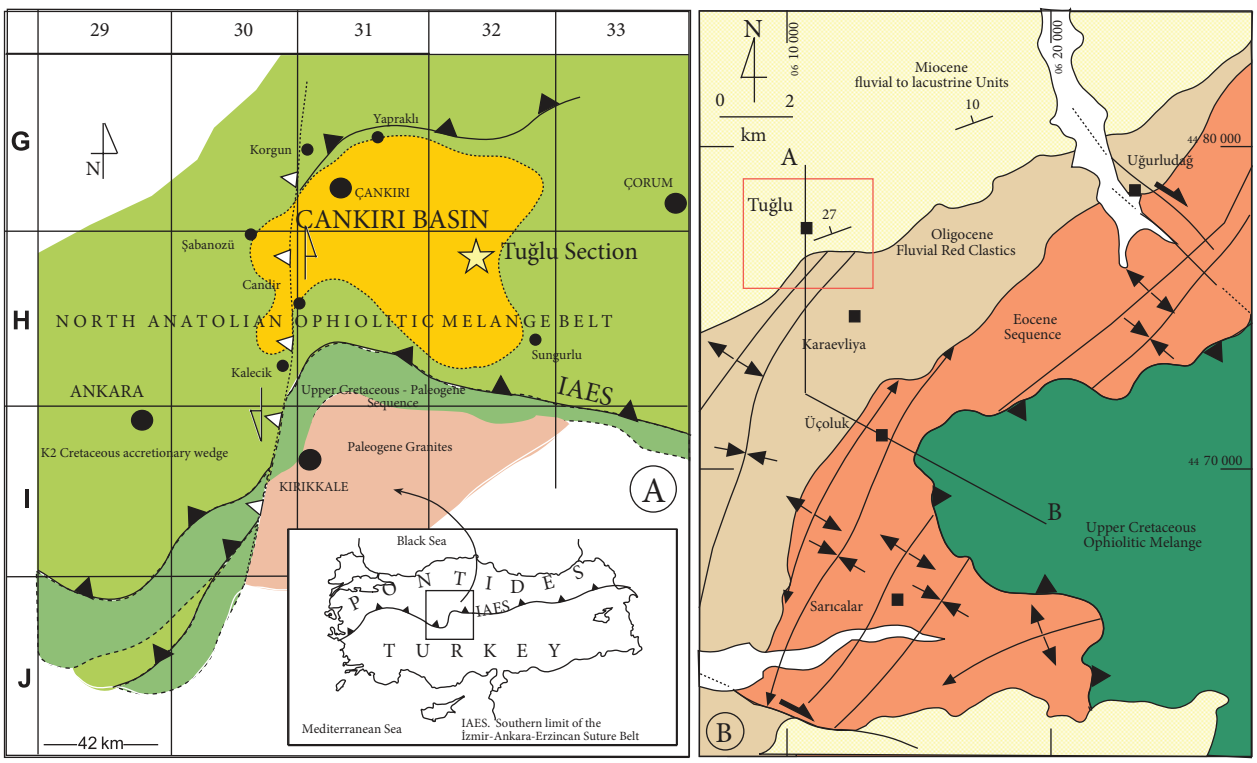


**Figure 1**. A) Location of the Çankırı Basin and the Tuğlu section (the orange colour indicates the area of the Çankırı Basin). B) Schematic geological map of the Tuğlu section area with undifferentiated Miocene deposits.

Anatolian-Dead Sea fault system in the south has resulted in an extensional regime in Anatolia since the Pliocene (Rotstein 1984; Kissel *et al*. 2003).

The Tuğlu section is located at 40°25′23.80″N, 34°18′44.40″E, immediately south of the village of Tuğlu (Figures 1B and 2). The section is exposed in an abandoned quarry, formerly exploited for lignite, and is about 25 m thick. The main lithology is silty clay, with 2 distinct sand layers at the bottom and at the top. Organic-rich intervals are quite common throughout the section, with lignite layers that are centimetres thin occurring in the lower part. The sequence is relatively undeformed at the outcrop scale, but the overly consolidated silty clays are densely fractured, also due to strong weathering processes (Figure 3). Field observations suggest that the succession was not affected by any significant diagenetic overprint. The high proportion of clay in the Tuğlu Formation likely prevented the succession from pervasive circulation of early diagenetic fluids and hence the growth of secondary carbonate. A deep burial diagenesis can be ruled out on the basis of low coalification ranks recorded in the basin: the calorific values are about 13,000 kJ/kg, corresponding to the lignite stage (C.A. Palmer *et al*. 2004).

Kaymakçı (2000: p. 102, Figure 4.14) described this section as the type section of the Tuğlu Formation, which he was the first to separate and distinguish from the Upper Oligocene Bayındır Formation (Birgili *et al*. 1975). Kaymakçı (2000) identified 2 unconformities bounding the Tuğlu Formation: the lower being the contact with the Çandır Formation, and the upper representing the contact with the Süleymanlı Formation. On the base of the small-mammal fauna recovered from several sections including Tuğlu, Kaymakçı attributed the Tuğlu Formation to the MN10 zone, corresponding to Middle Tortonian. From a palaeoenvironmental point of view, he interpreted the Tuğlu Formation as a fluvio-lacustrine facies with fluctuating water levels and rivers draining the system.

Karadenizli (2011: p. 14) assigned the Tuğlu section to the Bayındır Formation that he interpreted to be Late Miocene, rather than Late Oligocene, in age. He considered the lower boundary as conformable with the Kumartaş Formation (dated Early to Middle Miocene and corresponding to the Altıntaş Formation of Kaymakçı 2000). According to Karadenizli (2011), the upper boundary of the Süleymanlı Formation is conformable as well, except for local unconformities linked to syn-sedimentary tectonics. He recognised an alternation of massive mudstone and laminated claystone along the section. The massive mudstones were deposited in a fluvial to marsh environment, indicating decreased flooding

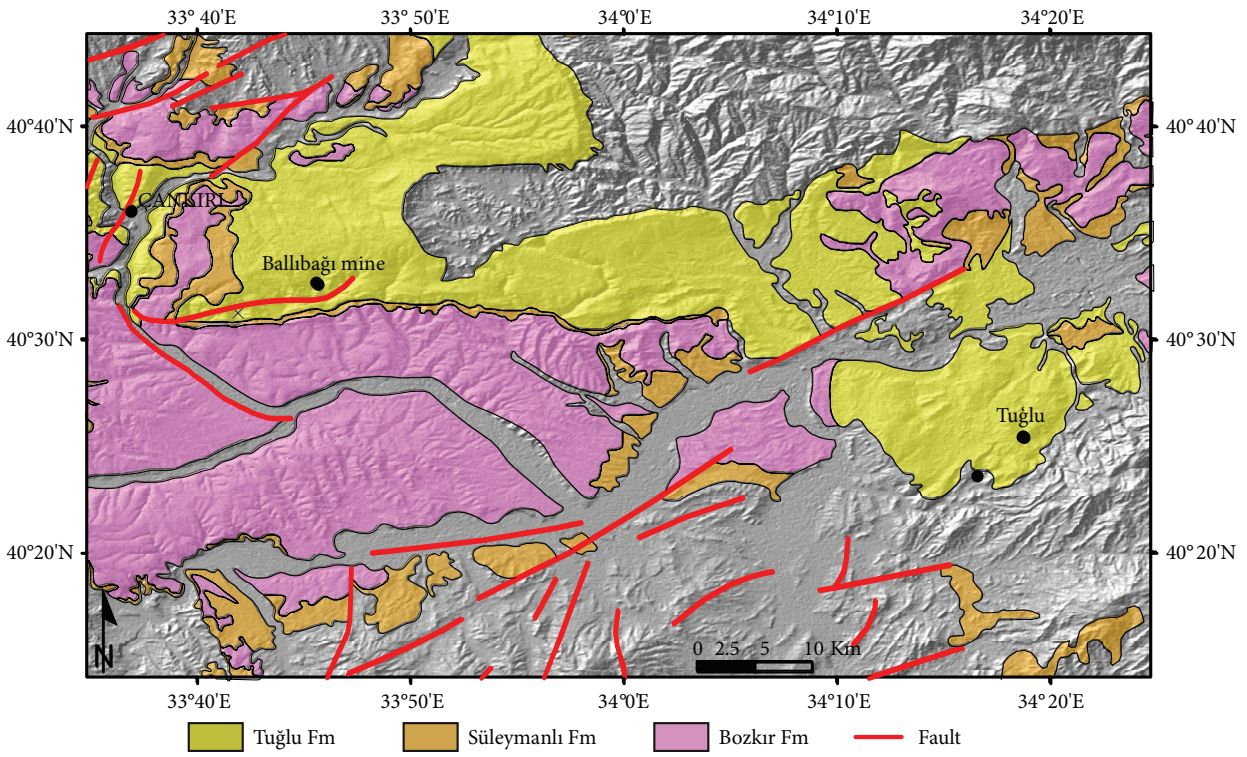


**Figure 2**. Geological map of the area modified after Kaymakçı *et al.* (2010) draped over shaded relief. Black dots indicate cited localities.

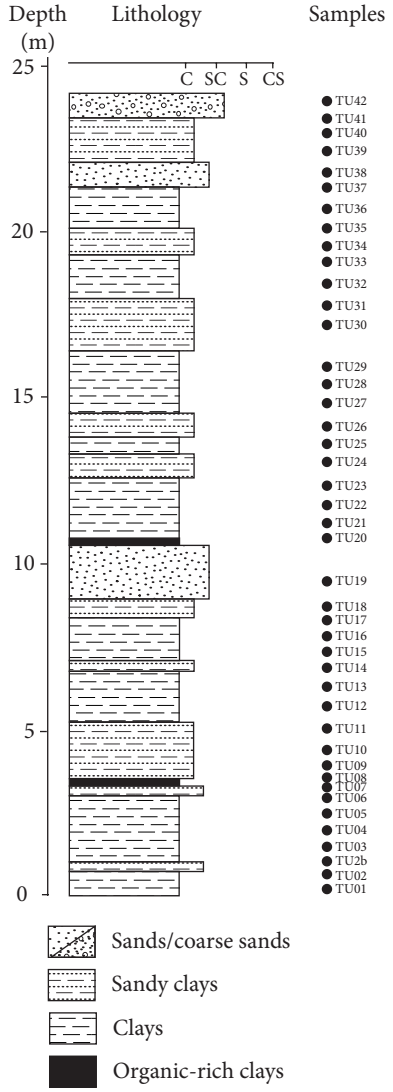


**Figure 3**. Stratigraphic column of the Tuğlu section. Lithostratigraphy and collected samples are shown.

frequency and predominant sedimentation from the suspended fraction. The laminated claystones represent a lacustrine environment and were deposited under a pluvial and mild climate.

## 3. Material and methods

The Tuğlu section has been sampled for a range of different analyses. Sampling took place in 4 consecutive field seasons from 2008 to 2011. The section revealed an unusual richness in both micro- and macrofossil content, such as molluscs, ostracods, and foraminifera. Less frequent but highly spectacular fossils include crab, turtle, fish, and plant remains.

### 3.1. Small mammals

Approximately 2 t of sediments were processed from each of 2 sampled layers (TU6/TU7 and TU19). The sediment was dried in the sun and subsequently sunk into plastic buckets filled with water for approximately 12 h. After soaking, the sediment was washed in the field on a set of sieves (0.5 mm and 2.5 mm mesh sizes). After drying of the residuum, the mammal remains were separated under a stereomicroscope. Some of the specimens were treated in an ultrasonic bath to be cleaned. The material of small mammals is housed in the collection of the Department of Geology and Palaeontology of Comenius University in Bratislava, Slovakia.

Approximately 400 teeth of small mammals were recovered from the 2 fossiliferous layers within the section. The rodent remains represent more than 300 cheek teeth: 190 cheek teeth and fragments of cheek teeth from TU19, and 123 teeth from TU6/TU7. A small part of material from layer TU6/TU7 (18 teeth and fragments) was provided by Hans de Bruijn (Utrecht, the Netherlands), who first discovered small mammals from this site in the late 1990s. The list of fauna recovered by Hans de Bruijn was published in Kaymakçı (2000).

### 3.2. Foraminifera and calcareous nannofossils

Foraminifera and calcareous nannofossils occur in the lowermost part of the section in the first 6 samples, TU1–TU6. For foraminifer analysis, approximately 200 g of sediment per sample was soaked, diluted, and disaggregated in water, and then washed under running water through 125 μm and 71 μm mesh sieves. Approximately 200 specimens from each sample were picked, identified, measured, and counted. Raw data were transformed into percentages of total abundance. Species with similar environmental significance were grouped to interpret their distribution patterns. Palaeoecological demands of the species used for estimation are based on published data (Murray 1973, 2006; Sgarrella & Moncharmont-Zei 1993; Meriç *et al*. 2004; Spezzaferri 2004; Hohenegger 2005).

Calcareous nannofossil assemblages were studied on smear slides prepared by standard techniques in order to study their abundance in areas with ideal distribution. The slides were examined under an Olympus X50 polarised light microscope at 1200× magnification.

### 3.3. Molluscs, charophyte gyrogonites, and ostracods

To achieve comprehensive palaeontological analyses on the whole exposed succession, 42 samples were taken over a stratigraphic thickness of 24 m (Figure 3). About 1 kg of sediment was first dried in an oven, then disaggregated with diluted hydrogen peroxide and washed on 1.25 mm and 0.63 mm mesh sieves.

Only 14 samples provided mollusc remains. The assemblages are composed of nonmarine gastropods (freshwater and terrestrial prosobranchs and pulmonates) and freshwater bivalves (Unionoida). Generally the shells are poorly preserved due to mechanical fragmentation in the depositional environment. In spite of careful sample

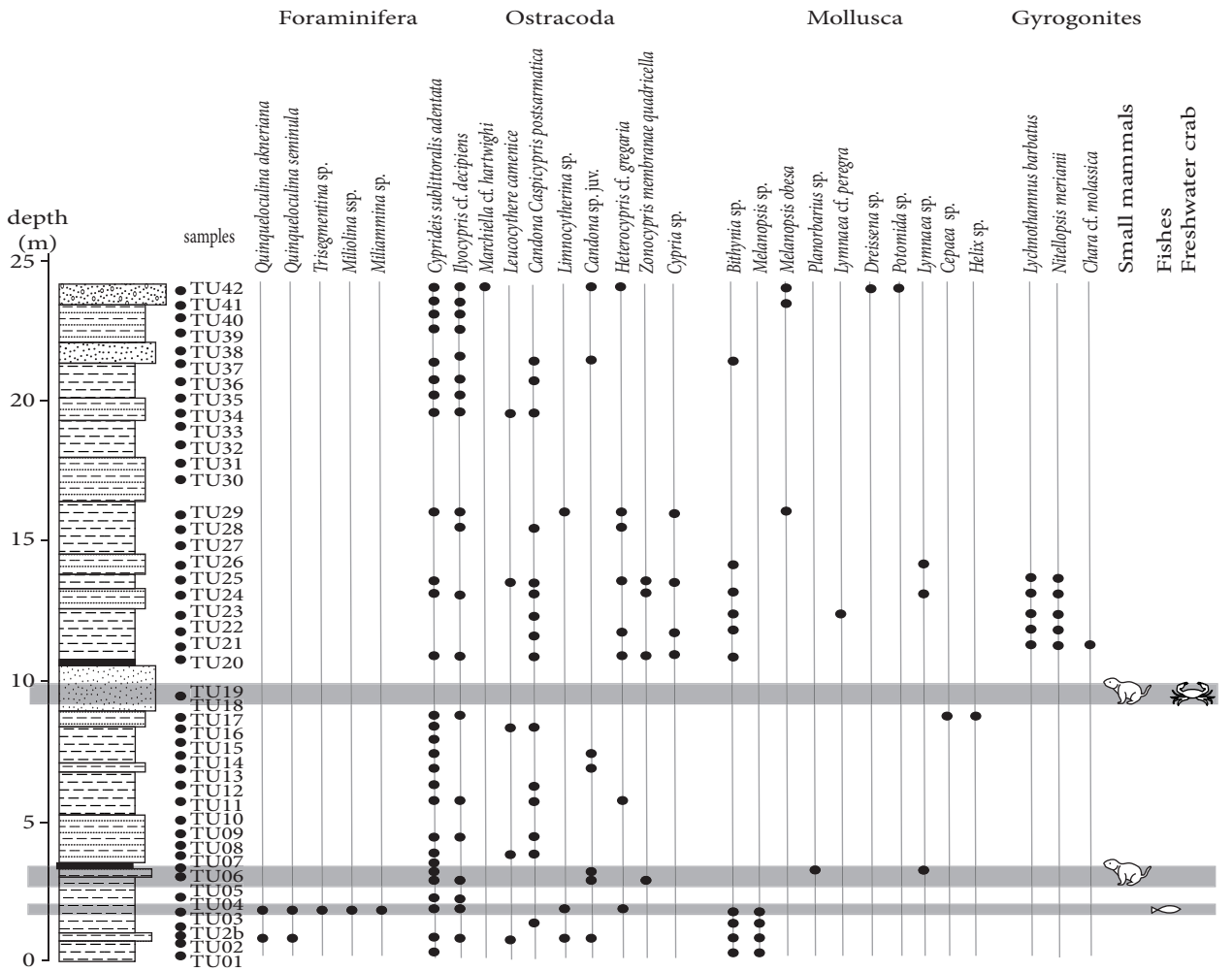


**Figure 4**. Stratigraphic column of the Tuğlu section, collected samples, and occurrence of fossils (foraminifera, ascidian spicules, ostracods, molluscs, gyrogonites, small mammals).

treatment in the laboratory (delicate washing, sieving, and low-temperature drying), it was not always possible to identify the molluscs at the species or genus level.

The charophyte remains from the Tuğlu section consist only of calcified oospores (termed gyrogonites). Occurrence of gyrogonites in the section is clearly restricted to the interval between samples TU21 and TU25.

Ostracods occur in 32 samples. They are relatively well preserved, although the percentage of broken valves is quite high, exceeding 50% in the samples from the lower part of the section. Whenever possible, at least 300 ostracod valves per sample were handpicked and identified under a stereomicroscope (Nikon SMZ-U, 15×–150×). Each species frequency was normalised to 10 g of dried sieved sample and the relative abundance (%) of each taxon was determined. Species represented only by juveniles or by single adult valves with occurrences of <10 were considered displaced valves (C population structure, sensu Whatley 1988; allochthonous low-energy taphocoenosis sensu Boomer *et al*. 2003). Interpretation of the assemblages used autoecological data from the literature. The material is hosted in the micropalaeontological collection of the Geological Sciences Department at Roma Tre University, Rome, Italy.

### 3.4. Pollen and spores

Samples for pollen analysis were treated according to the modified Erdtman method using hydrofluoric and hydrochloric acid to remove any inorganic constituent

(Erdtman 1943). The application of heavy liquid ($ZnCl_2$) with 2 g/cm$^3$ density was used to increase the number of palynomorphs. The microscope slides were prepared using glycerine water as a mounting medium, and 1 to 3 slides from each sample were examined depending on the frequency of sporomorphs. All samples are housed in the micropalaeontological laboratory at the Department of Geology and Palaeontology, Comenius University in Bratislava.

Pollen and spores were identified under a Zeiss Axioskop 40 microscope at a magnification of 200× to 630×. Only 8 samples contained sufficient material. Data from all spore-pollen spectra were then used to construct a synthetic pollen diagram. The percentage of the vegetation units was calculated from the total sum of the determined pollen grains and spores using the POLPAL program (Walanus & Nalepka 1999). The total Palaeotropical/Arctotertiary ratio (P/A) and individual palaeotropical and arctotertiary geofloristic elements are classified according to Mai (1991) and Ziembińska-Tworzydło *et al*. (1994a, 1994b), vegetation unit terminology, and classification sensu Kovar-Eder *et al*. (2008). Nonarboreal and arboreal pollen ratio (NAP/AP) is used to explain the main vegetation and landscape character. In order to obtain quantified climatic data, pollen data were subjected to the coexistence approach (CA) proposed by Mosbrugger and Utescher (1997). The CA method is based on the nearest living relative (NLR) with the presumption that climatic requirements of Tertiary plants are similar to those of their NLRs. The aim of the CA is to find intervals of various climate parameters for a given fossil flora in which a maximal number of NLRs of this fossil flora can coexist.

**3.5. Palaeomagnetism**

Samples were collected using a gasoline-powered portable drilling apparatus with a water-cooled diamond bit. The cores were oriented with a magnetic compass. The palaeomagnetic and rock magnetism analyses were carried out at the palaeomagnetic laboratories of the Istituto Nazionale di Geofisica e Vulcanologia in Rome, Italy. The natural remanent magnetisation (NRM) of 28 standard specimens was measured on a 2G Enterprises DC-SQUIDs cryogenic magnetometer, installed within a magnetically shielded room. The NRM of one specimen per core was measured by means of progressive stepwise demagnetisation using alternating field (AF) procedures. Stepwise AF demagnetisation was carried out using a set of 3 orthogonal AF coils mounted in-line on the 2G Enterprises system with increments of 5–10 mT during the first steps, followed by steps of 20 mT up to 100 mT. In order to identify the main magnetic carriers in the Tuğlu Formation, we carried out a series of rock magnetic analyses on selected specimens. Hysteresis properties were measured on small fragments scraped off of 39 palaeomagnetic specimens, using a MicroMag alternating gradient magnetometer (AGM model 2900, Princeton Measurements Corporation) with a maximum applied field of 1 T. From hysteresis cycles, after subtraction of the paramagnetic high-field susceptibility after saturation, we calculated the coercive force ($B_C$), the saturation remanent magnetisation ($M_{RS}$), and the saturation magnetisation ($M_S$). Stepwise acquisition of an isothermal remanent magnetisation (IRM) and subsequent back-field magnetisation (both in a succession of fields up to 1 T) were also measured on the same fragments with the MicroMag AGM, and the remnant coercive force ($B_{CR}$) was computed from the back-field remagnetisation curves.

**3.6. Stable oxygen and carbon isotope geochemistry**

From each ostracod-bearing sample about 4 valves of *Cyprideis sublittoralis adentata* were hand-picked, gently rinsed in distilled water, dried at room temperature, and not subjected to any further chemical or ultrasonic pretreatment (cf. Jin *et al*. 2006). Clay host-rock sample powders were extracted from hand specimens by a fine diamond-cast steel drill using fresh, clean, and homogeneous sample surfaces avoiding any visible skeletal components. All samples were digested in orthophosphoric acid and analysed as $CO_2$ using a ThermoFinnigan Delta V and a MAT253 mass spectrometer at the Geological Institute, University of Hannover and at the Institute of Geosciences, University of Frankfurt, respectively. In both cases, they were operated in continuous flow mode and interfaced to a ThermoFinnigan GasBench II. Analytical procedures largely followed those given by Spötl and Vennemann (2003). Raw data were calibrated against the Carrara marble standard (provided by T. Vennemann) with size correction performed on a daily basis and the NIST SRM18 standard reference material was used for external quality control. All data are reported in the standard delta notation against the Vienna Pee Dee Belemnite standard (V-PDB). Analytical uncertainty is invariably better than 0.3‰ and typically better than 0.1‰ absolute (2σ). Carbonate proportion within the whole-rock samples was derived from standard-sample total peak area ratios and are precise to within 1% absolute.

**3.7. Strontium isotope analysis**

$^{87}Sr/^{86}Sr$ isotope ratios of single *Cyprideis sublittoralis adentata* valves and tests of the benthic foraminifera Miliolidae were determined in situ using laser ablation multicollector inductively coupled plasma mass spectrometry (LA-MC-ICPMS) at the Institute of Geosciences, University of Frankfurt, following the procedure given by Mikes *et al*. (2011). This in situ, time-resolved analytical approach was adopted in preference to the conventional solution-based work due to the small sample amount available, the need to recognise possible

reworking, and the occasional presence of thin, Rb-bearing clay films on the valves. The analytical setup consisted of a ThermoFinnigan Neptune MC-ICPMS interfaced to a Resonetics RESOlution M-50 excimer LA instrument (λ = 193 nm), operated at 8 Hz repetition rate, 3.5 J/cm$^2$ energy flux, and dynamic ablation mode with variable, sample-dependent pit diameters between 53 (ostracods) and 140 μm (foraminifera). Following correction for interference (Rb, Kr, Ca-dimers, and bivalent rare earth elements) and mass fractionation (using a $^{86}Sr/^{88}Sr$ ratio of 0.1194), $^{87}Sr/^{86}Sr$ isotope ratios were normalised against NIST SRM987. Analytical uncertainties of the reported $^{87}Sr/^{86}Sr$ isotope ratios are typically around 0.000030 and invariably below 0.000042

### 3.8. Total organic carbon concentration and major element composition of whole rock samples

Total organic carbon (TOC) analyses were performed in the IR laboratory of organic geochemistry of the Geological Institute, Slovak Academy of Sciences in Banská Bystrica, using a Ströhlein C-MAT 5500 automatic infrared detector. Approximately 0.05 g of sample was pulverised, dried at 110 °C, and combusted in an oxygen atmosphere in a temperature range of 50–1000 °C. The $CO_2$ liberated during combustion was detected by a C-MAT 5500 infrared detector and recast to total carbon content (TC). Another split of sample was treated with hot HCl to dissolve any carbonate. The insoluble residue was analysed to obtain total organic carbon content (TOC). The total inorganic carbon (TIC) was calculated as follows: TIC = TC – TOC. The accuracy of measurements was controlled with certified international reference materials. Net analytical precision is about 0.08 wt.% absolute in the range of the measured concentrations.

The major element composition of 6 selected samples (samples TU1, TU3, TU21, TU23, TU35, and TU39) was determined on pressed powder pellets by energy-dispersive X-ray fluorescence technique using a SPECTRO X-LAB 2000 spectrometer in the Geoanalytical Laboratory at the State Geological Institute of Dionýz Štúr in Spišská Nová Ves, Slovakia. Analytical precision is typically within 5%.

## 4. Results

### 4.1. Composition of the rodent assemblages

Two large sediment samples (from samples TU6/TU7 and TU19, Figure 4) were processed for obtaining small mammal remains.

The assemblages of small mammals from both layers differed in composition considerably. The assemblage of rodents from the lower layer (samples TU6/TU7) consisted of 123 teeth and fragments of teeth and was represented by *Myomimus dehmi* (31%), *Megacricetodon* cf. *collongensis* (49%), *Progonomys cathalay* (12%), and *Byzantinia bayraktepensis* (8%). The rodent assemblage from upper layer 19 consisted of *Megacricetodon* sp. (7%), *Myocricetodon* sp. (1%), *Byzantinia bayraktepensis* (59%), *Byzantinia* sp. (4%), *Myomimus dehmi* (15%), *Myomimus* sp. (1%), *Microdyromys complicatus* (2%), *Myoglis ucrainicus* (3%), *Muscardinus thaleri* (2%), *Spermophilinus bredai* (4%), and *Keramidomys* sp. (3%). The percentages shown above for each taxon represent the proportion of lower and upper first and second molars for each species with respect to the total number of lower and upper first and second molars. The assemblage from layer 6/7 was dominated by taxa considered to be adapted to drier and more open environmental conditions (69%). The composition of the assemblage from sample TU19 was similar in terms of ecological preferences, but with a more diversified fauna. These results are in agreement with the general increasing trend observed in species diversity in Anatolian mammal assemblages during the time interval MN7/8–MN12 (Fortelius *et al*. 1996).

### 4.2. Foraminifera

Miliolidae foraminifera occurred in the lowermost part of the section, from sample TU1 to sample TU6. Sample TU1 contained *Quinqueloculina* sp. and *Miliolina* sp. with normal size and coiling in low abundances (5 specimens/0.5 g residuum). Samples TU2, TU2b, and TU3 lacked any autochthonous foraminifera, and only Cretaceous reworked species of *Globotruncana* sp. were identified. Sample TU4 contained a residuum very rich in specimens of the genera *Miliolina*, *Quinqueloculina*, *Trisegmentina*, *Varidentella*, and *Miliammina*, with approximately 99% of clasts consisting of porcellaneous foraminifera shells (Figure 4; Plate 1), with abnormal coiling and large diameter (more than 2000/0.5 g residuum). Samples TU5 and TU6 contained a large amount of small, thin-walled porcellaneous species in a very fine residuum. Shell preservation in sample TU6 was extremely poor.

### 4.3. Calcareous nannoplankton

Calcareous nannofossil assemblages were exclusively represented by redeposited Palaeogene species (*Coccolithus pelagicus*, *Cyclicargolithus floridanus*, *Sphenolithus radians*, *Sphenolithus* sp., *Zygrhablithus bijugatus*, *Reticulofenestra* spp., *Discoaster* spp.) and rare Cretaceous species (*Eiffellithus* spp., *Micula staurophora*, *Prediscosphaera cretacea*). These forms occur in several samples (TU1–2, TU5, TU16, TU18–26, TU34). Fossil didemnid ascidian spicules of various shapes were found in many samples (TU1–4, TU5, TU16, TU18–30, TU34). They are particularly abundant in the set of samples TU1 to TU4. Identified spicules included *Rigaudia multiradiata*, *Mirascidites vulgaris*, and *Mirascidites paucivulgaris*.

### 4.4. Ostracods

Ostracods occurred in 32 samples, with 10 different species (Figure 4; Plate 2). The dominant species was *Cyprideis*

*sublittoralis adentata* Bassiouni 1979, which occurred in 28 samples and outnumbered the other species for number of specimens in each sample. It constituted 93% of the specimens. The second most common species was *Ilyocypris* cf. *decipiens*, always occurring together with *C. sublittoralis adentata*. When *C. sublittoralis adentata* was scarce, *Ilyocypris* cf. *decipiens* became the dominant species. In such intervals, the accompanying species were *Leucocythere camenice*, *Limnocytherina* sp., *Marchiella* cf. *hartwigi*, *Candona* sp. juv., and *Candona* (*Caspiocypris*) *postsarmatica*. The latter became dominant when both *Cyprideis* and *Ilyocypris* were absent or represented mostly by juveniles. The assemblage then included *Heterocypris* cf. *gregaria*, *Zonocypris membranae quadricella*, and *Cypria* sp.

**4.5. Molluscs**

Molluscs occurred dispersed throughout the sedimentary succession (Figure 4). They were terrestrial and freshwater (or low-oligohaline) gastropods and bivalves, for a total of 10 identified taxa. At the base, the few remains of freshwater taxa were clearly transported, whereas all other identified taxa were considered in situ. In sample TU18, many crushed shells of terrestrial gastropods of the family Helicidae, belonging only to the 2 genera, *Cepaea* Held and *Helix* Linnaeus, were recognised in a coarse matrix. In sample TU23, an abundant freshwater gastropod assemblage was recorded, with *Lymnaea* cf. *peregra* Müller and *Bithynia* sp. being dominant. Even if it is among the richest assemblages of the section, it was possible to recognise only the 2 mentioned taxa, due to the very poor state of the shells. In sample TU42, an oligotypic assemblage very rich in specimens of freshwater taxa was recorded. The assemblage consisted of *Melanopsis obesa* and poorly preserved fluviatile bivalves with disarticulated valves, such as *Dreissena* sp. and *Potomida* sp., in which the nacreous layer typical of this genus was visible in the internal side (Plate 3).

**4.6. Charophyte gyrogonites**

The charophyte remains consisted of the calcified oospores of 3 species: *Nitellopsis merianii* (A. Braun ex Unger 1850) Grambast & Soulié-Märsche 1972, *Lychnothamnus barbatus* (Meyen) v. Leonhardi 1863 var. *antiquus* nov. var. Soulié-Märsche 1989, *Chara* cf. *molassica* Straub 1952 (Plate 4). The gyrogonites were strictly limited to the portion between samples TU21 and TU25 (Figure 4).

**4.7. Pollen and spores**

Riparian forests with *Ulmus*, *Alnus*, and *Salix* and local coastal swamps with the dominant *Glybtostrobus* (Cupressaceae, subf. Taxodioidea), Myricaceae, and Thyphaceae represented the azonal vegetation. In the pollen spectra, zonal vegetation with rare *Quercus*, *Pterocarya*, Oleaceae, *Engelhardia*, *Carya*, *Ephedra*, Ericaceae, and highly abundant nonaquatic herbs of Asteraceae was present, dominated by Poaceae grasses and the saline- and drought-tolerant Chenopodiaceae from the family Amarathaceae. The subdominant steppic element *Artemisia* also commonly occurred in this association (Figure 5A).

The increased proportion of 15%–20% Pinaceae pollen was noticeable in the upper part of the profile, reaching the maximum value of 30% at the top of it. There was a strong nonarboreal pollen dominance visible based on the NAP/AP ratio (Figure 5B). This is represented by the high percentage of herbs and shrubs in the pollen spectra, which reflects an open grassland landscape with local forests (Figure 5A). The palaeotropical and arctotertiary geofloristic element proportion calculation was applied to the mesophytic taxa and showed that palaeotropical taxa prevailed in the entire profile. The total P/A ratio, including azonal vegetation, reflected the dominance of warm temperate geofloristic elements (Figure 5C). Both semiquantitative analysis results indicated a subtropical, warm temperate climate where the Tuğlu Formation was deposited.

Based on the CA analysis sensu Mosbrugger and Utescher (1997), the mean annual temperature and mean annual precipitation in the Tuğlu section in the studied profile varied in coexistence intervals of 13.8–17 °C and 823–932 mm/year. Precipitation in the driest month varied between 9 and 45 mm and the temperature of the coldest month between 3.1 and 10.3 °C coexistence interval.

**4.8. Other fossils**

The Tuğlu section samples yielded several other fossil taxa. The lower part of the Tuğlu section (sample TU4) yielded otoliths of the fish genus *Aphanius* (Plate 1). In sample TU19, chelae of potamid crabs were identified and assigned to the genus *Potamon*.

**4.9. Stable oxygen and carbon isotopes**

Whole-rock stable carbon and oxygen isotope records are linked to the carbonate content of the samples, which mostly varies between 5 and 20 wt.% (Figure 6A). In the analysed samples, carbonate contribution from fragmented skeletal components (such as ostracods or molluscs, as well as reworked nannofossils) cannot be generally excluded. However, the fine-grained, homogeneous, and clay-rich lithology strongly suggests that the bulk of the carbonate was precipitated as fine-grained intrabasinal particles, most likely via abiotic processes and/or algal bioproductivity in the epilimnion. Furthermore, in agreement with field observations, macroscopic examination of the samples revealed there was no sparry carbonate present. The stable isotopic composition and carbonate proportion of 46 whole-rock samples, along with 25 ostracod samples of adult *Cyprideis sublittoralis adentata* valves are listed in Tables 1 and 2 and plotted in Figures 6A and 6B. $\delta^{18}O$ values of the silty clays vary in a relatively restricted range

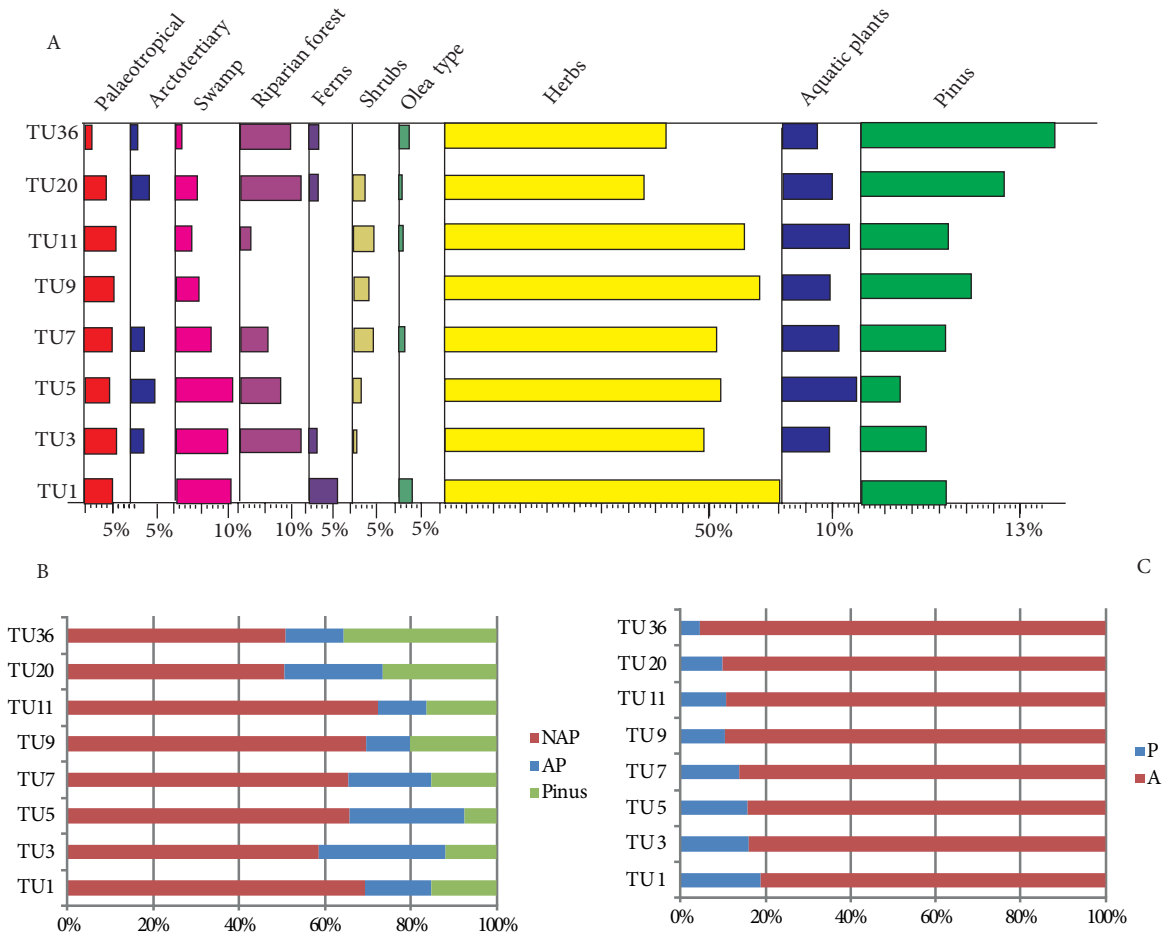


**Figure 5**. A) Palaeoecological groups based on pollen analysis; B) proportion of nonarboreal and arboreal pollen with excluded *Pinus* (NAP/AP); C) palaeotropical and Arctotertiary geofloristic element ratio (P/A ratio) (sample distances are not in scale).

between –6.3 and –3.9‰ (median value: –5.0‰), with $\delta^{13}C$ displaying a higher variability between –13.1 and –5.1‰ (median value: –8.5‰). A mild negative excursion of approximately 1‰ in both $\delta^{18}O$ and $\delta^{13}C$ is observed between the top of the interval C and the base of the interval F.

The $\delta^{18}O$ and $\delta^{13}C$ values of the ostracod valves vary from –5.1 to –1.7‰ and from –10.2 to –5.2‰, respectively, and in the lowermost 3 m of the section they indicate relatively high-frequency fluctuations as compared to the host silty clays. Ostracod $\delta^{18}O$ values are less negative than their host sediment and display a variable but consistently present offset of up to 2.5‰.

### 4.10. Total organic carbon concentration and major element composition of whole-rock samples

The sediments are silty clays with a carbonate proportion of typically 5 to 20 wt.% (median value: 12 wt.%). TOC concentrations uniformly decrease from the base of the profile until the middle part of interval C, from about 0.4 down to 0.1 wt.%. In a further up section, there is a reversed, increasing trend of TOC concentrations reaching approximately 0.3 wt.% at the top of the profile, whereas this increase is accompanied by a higher variability of the organic matter content (Figure 6A; Table 3).

Silicate-bound molar $Al_2O_3$, $K_2O$, $Na_2O$, and CaO were used to calculate the chemical index of alteration (CIA; Nesbitt & Young 1982, 1984) for 6 silty clay samples, the most widely applied major element proxy for chemical weathering. As shown in Figure 6C, CIA values range from 66 to 75 (averaging about 70), indicating a largely granodioritic sediment source and only a moderate degree of chemical weathering in the hinterland (Table 4). It should be noted, however, that since even slight natural grain size variations exert a strong control on CIA variability, the extent of the data array likely exceeds the real intersample variation in the recorded weathering intensity (Armstrong-Altrin & Verma 2005; Tolosana-Delgado 2012; von Eynatten *et al.* 2012).

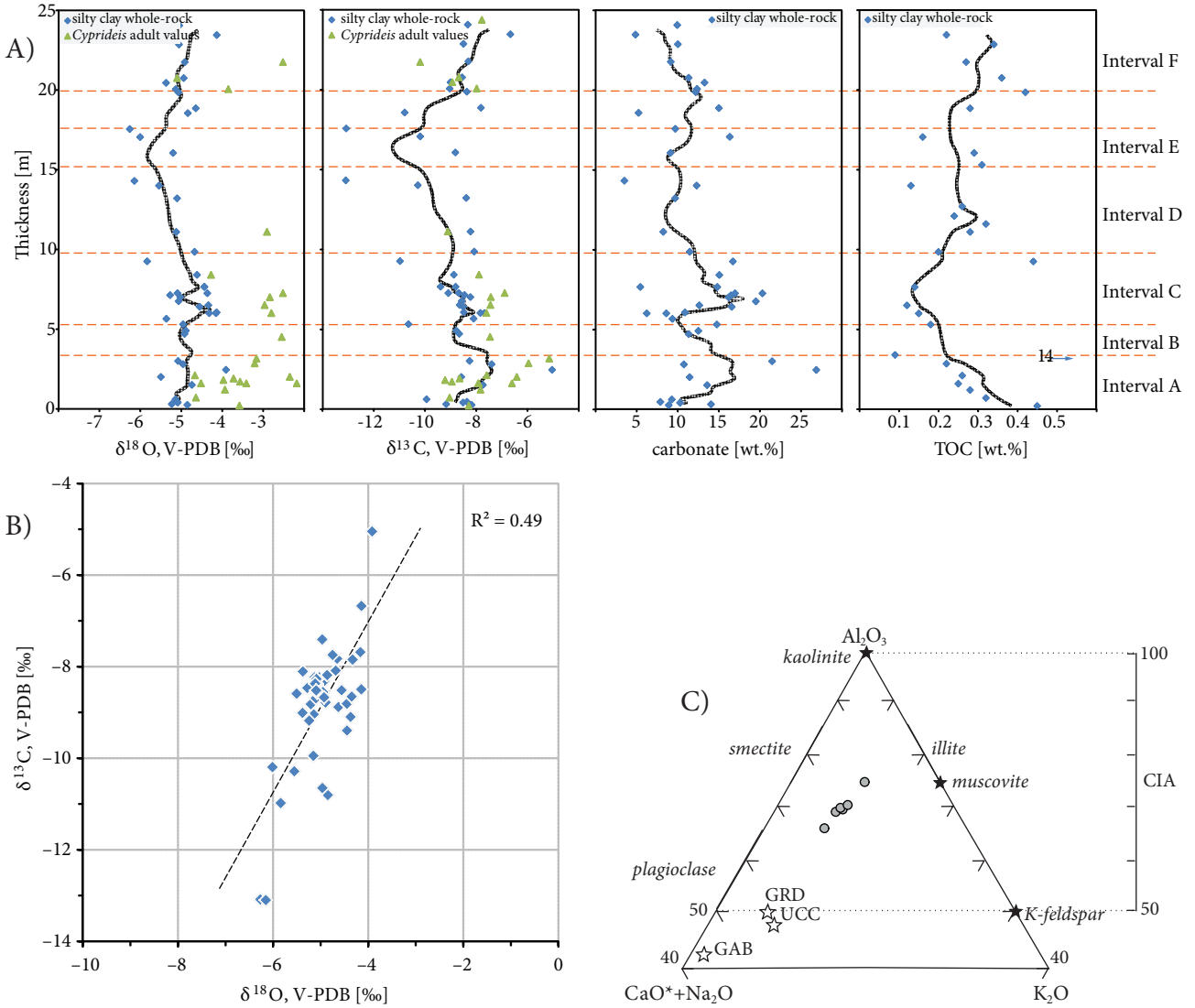


**Figure 6**. A) Panels from left to right: oxygen isotopic composition of adult *Cyprideis sublittoralis adentata* valves and the host silty clays; carbon isotopic composition of adult *Cyprideis sublittoralis adentata* valves and the host silty clays; carbonate concentrations of the host silty clays; total organic carbon concentrations of the host silty clays – all plotted against stratigraphy. Grey curves: 5-point running averages of whole-rock analytical data. Horizontal dashed lines separate distinct intervals as revealed by palaeoenvironmental analysis. B) Carbon versus oxygen isotopic composition of the host silty clays. C) A-CN-K plot with molar values, indicating CIA values (Nesbitt & Young 1984) for the Tuğlu Formation silty clays. CaO* is silicate-bound CaO, estimated to represent 10% of the total $Na_2O$ content. The apparent linear trend towards illite likely results from grain-size effects (cf. von Eynatten *et al.* 2012). Asterisks show average UCC composition (Taylor & McLennan 1985) and average granodiorite (GRD) and gabbro (GAB) compositions (Le Maitre 1976).

### 4.11. $^{87}Sr/^{86}Sr$ isotope ratios

Individual $^{87}Sr/^{86}Sr$ isotope ratios of 8 *Cyprideis sublittoralis adentata* valves and 2 Miliolidae tests from throughout the profile are shown in Figure 7 and Table 5. Overall, the $^{87}Sr/^{86}Sr$ ratios are invariably low and range from 0.707129 ± 0.000029 to 0.707677 ± 0.000025, and they likely indicate 2 significant groupings. At the base of the profile, in intervals from A to base C, the $^{87}Sr/^{86}Sr$ ratios are the lowest at about 0.7072, whereas in interval F, likewise low yet characteristically different $^{87}Sr/^{86}Sr$ ratios are encountered that range from 0.7076 to 0.7077. Two valves from a single sample yield markedly different compositions in interval E. With respect to the density of the data, the foraminifera and the ostracods in the lower part of the section are indistinguishable in terms of their Sr isotopic composition.

**Table 1.** Silty clay whole-rock $\delta^{18}O$, $\delta^{13}C$, and carbonate concentration data.

| Sample | Thickness (m) | $\delta^{18}O_{V\text{-}PDB}$ (‰) | $\delta^{13}C_{V\text{-}PDB}$ (‰) | Carbonate wt.% |
|---|---|---|---|---|
| TU41 | 24.05 | –5.06 | –8.34 | 9.9 |
| TU40 | 23.45 | –4.14 | –6.68 | 4.9 |
| TU39 | 22.85 | –5.06 | –8.51 | 10.0 |
| TU37 | 21.75 | –4.92 | –8.32 | 9.1 |
| TU36 | 20.75 | -4.95 | –8.56 | 11.3 |
| TU35 | 20.45 | –5.38 | –9.01 | 13.3 |
| TU34 | 20.05 | –5.14 | –9.04 | 12.4 |
| TU33 | 19.85 | –5.08 | –8.37 | 12.2 |
| TU32 | 18.85 | –4.65 | –7.83 | 15.0 |
| TU31 | 18.55 | –4.85 | –10.80 | 5.2 |
| TU30 | 17.55 | –6.27 | –13.08 | 9.7 |
| TU29 | 17.05 | –6.01 | –10.20 | 16.3 |
| TU28 | 16.05 | –5.21 | –8.82 | 9.1 |
| TU26 | 14.30 | –6.15 | –13.10 | 3.5 |
| TU25 | 14.00 | –5.55 | –10.29 | 12.3 |
| TU24 | 13.20 | –5.11 | –8.40 | 9.7 |
| TU20 | 11.10 | –5.13 | –8.23 | 8.2 |
| TU19 | 9.85 | –4.68 | –8.09 | 11.5 |
| TU18 | 9.25 | –5.84 | –10.98 | 16.7 |
| TU17 | 8.40 | –4.62 | –8.88 | 15.1 |
| 09TU32 | 7.65 | –4.44 | –9.40 | 5.4 |
| TU16 | 7.65 | –4.45 | –8.81 | 14.8 |
| 09TU31 | 7.25 | –5.10 | –8.69 | 17.0 |
| TU15 | 7.25 | –4.37 | –9.10 | 20.3 |
| 09TU29 | 7.13 | –5.28 | –8.47 | 16.5 |
| TU14 | 7.00 | –5.03 | –8.23 | 16.2 |
| 09TU28 | 6.75 | –5.07 | –8.57 | 19.5 |
| TU13 | 6.50 | –4.35 | –8.66 | 12.6 |
| 09TU27 | 6.40 | –4.56 | –8.52 | 16.6 |
| 09TU26 | 6.05 | –4.14 | –8.49 | 10.9 |
| 09TU25 | 6.00 | –4.33 | –7.85 | 8.6 |
| TU12 | 6.00 | –4.16 | –7.68 | 6.2 |
| 09TU22 | 5.65 | –5.37 | –8.11 | 9.4 |
| TU11 | 5.30 | –4.96 | –10.65 | 14.8 |
| 09TU18 | 4.90 | –4.89 | –8.78 | 12.5 |
| 09TU17 | 4.70 | –4.93 | –8.67 | 11.3 |
| 09TU16 | 3.00 | –5.08 | –8.27 | 21.5 |
| 09TU14 | 2.80 | –4.97 | –7.41 | 10.7 |
| 09TU11 | 2.45 | –3.92 | –5.05 | 26.9 |
| 09TU10 | 2.00 | –5.50 | –8.59 | 11.5 |
| 09TU08 | 1.50 | –4.75 | –7.74 | 13.6 |
| 09TU05 | 0.60 | –5.15 | –9.95 | 9.3 |
| 09TU04 | 0.45 | –5.12 | –8.37 | 7.9 |
| 09TU03 | 0.40 | –5.09 | –8.52 | 10.3 |
| 09TU02 | 0.30 | –5.24 | –9.18 | 14.1 |
| 09TU01 | 0.25 | –4.86 | –8.19 | 8.9 |

**Table 2.** $\delta^{18}O$ and $\delta^{13}C$ data of adult *Cyprideis sublittoralis adentata* valves.

| Sample | Thickness (m) | $\delta^{18}O_{V\text{-}PDB}$ (‰) | $\delta^{13}C_{V\text{-}PDB}$ (‰) | No. of valves | Weight (μg) |
|---|---|---|---|---|---|
| TU42V | 24.35 | –1.95 | –7.79 | 5 | 188 |
| TU37V | 21.75 | –2.52 | –10.20 | 4 | 131 |
| TU36V | 20.75 | –5.11 | –8.69 | 3 | 117 |
| TU35V | 20.45 | –1.70 | –8.94 | 5 | 171 |
| TU34V | 20.05 | –3.86 | –7.99 | 4 | 145 |
| TU20V | 11.10 | –2.91 | –9.12 | 5 | 148 |
| TU17V | 8.40 | –4.28 | –7.90 | 5 | 165 |
| TU15V | 7.25 | –2.52 | –6.90 | 4 | 106 |
| TU14V | 7.00 | –2.84 | –7.44 | 3 | 113 |
| TU13V | 6.50 | –2.97 | –7.45 | 4 | 144 |
| TU12V | 6.00 | –2.81 | –7.61 | 1 | 41 |
| TU10V | 4.50 | –2.55 | –7.47 | 6 | 172 |
| TU7V | 3.15 | –3.17 | –5.16 | 5 | 145 |
| TU6V | 2.85 | –3.21 | –5.96 | 5 | 198 |
| TUHR21V | 2.10 | –4.68 | –7.60 | 5 | 196 |
| TUHR20V | 2.00 | –2.36 | –6.42 | 4 | 160 |
| TUHR19V | 1.90 | –3.73 | –8.66 | 3 | 105 |
| TUHR18V | 1.80 | –3.98 | –9.22 | 3 | 156 |
| TUHR17V | 1.70 | –3.57 | –8.96 | 4 | 190 |
| TUHR16V | 1.60 | –2.19 | –6.61 | 4 | 180 |
| TUHR16CV | 1.60 | –4.53 | –7.91 | 4 | 142 |
| TU4V | 1.60 | –3.42 | –7.93 | 4 | 157 |
| TUHR12V | 1.20 | –3.94 | –7.84 | 4 | 190 |
| TU2V | 0.70 | –4.65 | –9.05 | 3 | 92 |
| TU1V | 0.20 | –3.59 | –8.30 | 6 | 221 |

**4.12. Environmental magnetism**

Results from AF demagnetisation of the samples show that they have maximum values of NRM around 26.3 × $10^{-3}$ A/m. The intensity of magnetisation gently drops during the first 5 or 6 demagnetisation steps (up to 30–40 mT), and it is almost completely removed between 60 and 100 mT. In just a few cases the samples are not completely demagnetised at the end of the demagnetisation process. All samples show a single stable component of magnetisation with a normal polarity.

We performed mineralogical analyses of 39 samples collected along the whole section of 0–25 m (Figure 8). The average mean magnetic susceptibility (κ) is about 200 × $10^{-6}$ SI, which is typical for clays with a low content of ferromagnetic (sensu lato) minerals, whose susceptibility and magnetic fabric are controlled by the paramagnetic contribution in the clay matrix (Rochette 1987; Sagnotti 1998). Figure 8a shows that the susceptibility values are stable in the lower and the upper part of the section (intervals A and F), whereas they are variable along the section within intervals B, C, and D.

Hysteresis loops and IRM curves show that magnetite and hematite (or a mixture of them) are the main magnetic carriers in this sediment. These ferromagnetic minerals show 2 different granulometries: multidomain (MD) and a mixture of pseudo-single domain and MD (Day *et al.* 1977; Dunlop 2002; Dunlop *et al.* 2006).

Figure 8 shows the variation of the magnetic susceptibility, $IRM_{-100}$/SIRM (S ratio; IRM acquired with a back-field of 100 mT), $IRM_{-300}$/SIRM (S ratio; IRM acquired with a back-field of 300 mT), Mrs/Ms (remanence ratio), and Bcr/Bc (coercivity ratio) along the sampled section. All of these parameters, as already described for the magnetic susceptibility, record a sensible

**Table 3**. Organic carbon analyses: TC = total carbon, TOC = total organic carbon, TIC = total inorganic carbon, $CaCO_3$ = $CaCO_3$ %, n.d. = not detected.

| Sample | Thickness (m) | TC (wt. %) | TOC (wt. %) | TIC (wt. %) | $CaCO_3$ (wt. %) |
|---|---|---|---|---|---|
| TU40 | 23.45 | 1.20 | 0.22 | 0.98 | 8.17 |
| TU39 | 22.85 | 1.54 | 0.34 | 1.20 | 10.00 |
| TU37 | 21.75 | 1.54 | 0.27 | 1.27 | 10.58 |
| TU36 | 20.75 | 1.73 | 0.36 | 1.37 | 11.41 |
| TU33 | 19.85 | 2.02 | 0.42 | 1.60 | 13.33 |
| TU32 | 18.85 | 2.13 | 0.28 | 1.85 | 15.41 |
| TU29 | 17.05 | 2.91 | 0.16 | 2.75 | 22.91 |
| TU28 | 16.05 | 1.30 | 0.29 | 1.01 | 8.42 |
| TU27 | 15.30 | 0.32 | 0.31 | n.d. | n.d. |
| TU25 | 14.00 | 1.26 | 0.13 | 1.13 | 9.42 |
| TU23 | 12.70 | 0.28 | 0.26 | n.d. | n.d. |
| TU22 | 12.10 | 0.77 | 0.24 | 0.53 | 4.42 |
| TU21 | 11.60 | 0.50 | 0.32 | 0.18 | 1.50 |
| TU20 | 11.10 | 1.42 | 0.28 | 1.14 | 9.50 |
| TU19 | 9.85 | 1.74 | 0.20 | 1.54 | 12.83 |
| TU18 | 9.25 | 2.96 | 0.44 | 2.52 | 20.99 |
| TU16 | 7.65 | 2.40 | 0.14 | 2.26 | 18.83 |
| TU13 | 6.50 | 2.13 | 0.12 | 2.01 | 16.75 |
| TU12 | 6.00 | 1.78 | 0.15 | 1.63 | 13.58 |
| TU11 | 5.30 | 1.78 | 0.18 | 1.60 | 13.33 |
| TU8 | 3.40 | 0.09 | 0.09 | n.d. | n.d. |
| TU7 | 3.15 | 1.48 | 1.43 | n.d. | n.d. |
| TU6 | 2.85 | 6.26 | 0.22 | 6.04 | 50.32 |
| TU5 | 2.10 | 2.59 | 0.26 | 2.33 | 19.41 |
| TU4 | 1.60 | 3.21 | 0.25 | 2.96 | 24.66 |
| TU3 | 1.20 | 1.43 | 0.28 | 1.15 | 9.58 |
| TU2 | 0.70 | 1.88 | 0.32 | 1.56 | 13.00 |
| TU1 | 0.20 | 1.91 | 0.45 | 1.46 | 12.16 |

variation through the studied intervals along the section (Figure 8). In particular $IRM_{-100}$/SIRM and $IRM_{-300}$/SIRM are indicators of the higher relative contribution of the hard magnetic minerals, such as hematite, to the sample remanence; and Mrs/Ms and Bcr/Bc are the hysteresis parameters that indicate magnetic and granulometries differences in the sediments. Variation of these parameters are clearly recognisable along the studied section. See Section 5 for interpretation.

## 5. Discussion

### 5.1. Age of the Tuğlu section: biostratigraphic constraints and stable oxygen isotope records

The rodent assemblages collected from 2 separate layers refine the knowledge based on the previously published fauna and point to an age of the Tuğlu section that is older than proposed so far (Kaymakçı 2000; Karadenizli 2011). The occurrence of *Progonomys* in sample TU6/7 limits the age of the section to the Upper Miocene (Vallesian). The co-occurrence of relatively numerous *Megacricetodon* populations together with *Progonomys* is unusual. Occurrences of *Progonomys* together with *Megacricetodon* were reported so far from Pedregueras 2 C, Spain (Dam *et al.* 2001); Can Lobateres, Spain (Alberdi *et al.* 1981); and Castelnou 1B, France (Aguilar 1991). According to Wessels *et al.* (2001), the genus *Megacricetodon* occurs in at least 33 Turkish assemblages and ranges from MN3 (Keseköy) to MN7/8 (Yeni Eskihisar). Occurrences of *Megacricetodon* younger than MN7/8 are not currently known of in Turkey. The genus *Megacricetodon* disappeared from the

**Table 4**. Major element composition of selected silty clay samples derived by energy-dispersive X-ray fluorescence analysis. CaO*: silicate-bound molar CaO, assuming CaO* is 10% of the $Na_2O$ present. CIA: chemical index of alteration (Nesbitt & Young 1982, 1984).

| Sample | TU1 | TU3 | TU21 | TU23 | TU35 | TU39 |
|---|---|---|---|---|---|---|
| Concentration (wt.%) $SiO_2$ | 54.40 | 58.30 | 56.30 | 54.20 | 50.00 | 49.60 |
| $Al_2O_3$ | 15.00 | 15.30 | 16.70 | 17.30 | 13.80 | 14.90 |
| $Fe_2O_3$ | 7.20 | 7.46 | 8.81 | 9.36 | 7.24 | 7.91 |
| MgO | 3.52 | 2.55 | 3.79 | 4.25 | 4.13 | 4.60 |
| CaO | 5.03 | 2.75 | 1.59 | 0.93 | 7.96 | 6.51 |
| $Na_2O$ | 2.43 | 3.03 | 2.51 | 2.62 | 1.92 | 1.41 |
| $K_2O$ | 2.04 | 2.12 | 2.45 | 2.41 | 2.08 | 2.22 |
| $TiO_2$ | 0.91 | 0.89 | 0.90 | 0.88 | 0.81 | 0.84 |
| $P_2O_5$ | 0.13 | 0.12 | 0.20 | 0.16 | 0.20 | 0.18 |
| MnO | 0.07 | 0.04 | 0.07 | 0.05 | 0.13 | 0.06 |
| $SO_3$ | 0.22 | 0.32 | 0.30 | 0.32 | 0.20 | 0.39 |
| LOI | 8.72 | 6.84 | 6.13 | 7.23 | 11.20 | 11.00 |
| Total | 99.67 | 99.72 | 99.75 | 99.71 | 99.67 | 99.62 |
| Molar values | | | | | | |
| $Al_2O_3$ | 0.147 | 0.150 | 0.164 | 0.170 | 0.135 | 0.146 |
| CaO* | 0.004 | 0.005 | 0.004 | 0.004 | 0.003 | 0.002 |
| $Na_2O$ | 0.039 | 0.049 | 0.040 | 0.042 | 0.031 | 0.023 |
| $K_2O$ | 0.022 | 0.023 | 0.026 | 0.026 | 0.022 | 0.024 |
| CIA | 69.4 | 66.3 | 69.9 | 70.2 | 70.7 | 75.0 |

European fossil record during the Early Vallesian (MN9) (Fejfar *et al.* 2011). The first known record of *Progonomys* from Turkey comes from Sinap 108 (fragment of M1 and M2 of *Progonomys* sp.) (Sen 2003). This locality is dated MN9 (chron C5n2n) (Kappelman *et al.* 2003). The

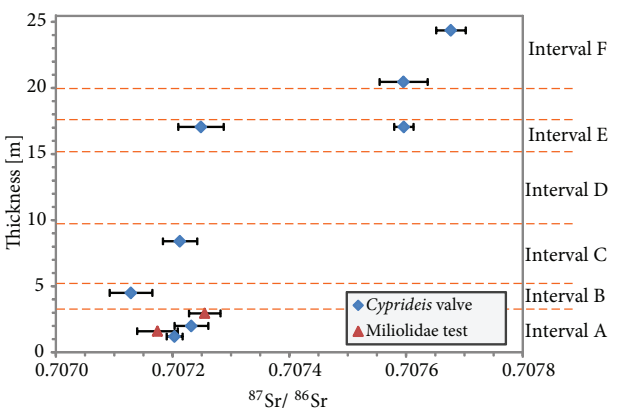


**Figure 7**. Stratigraphic distribution of $^{87}Sr/^{86}Sr$ ratios of single *Cyprideis sublittoralis adentata* valves and Miliolidae tests. Horizontal dashed lines separate distinct intervals as revealed by palaeoenvironmental analysis.

cooccurrence of *Megacricetodon* together with *Progonomys* in sample TU6/7 strongly suggests that the Tuğlu section can be correlated with the lower part of the Vallesian (early MN9). Thus, the Tuğlu locality represents the youngest occurrence of the genus *Megacricetodon* from Anatolia. It cannot be excluded that the occurrence of the genus *Progonomys* also represents one of the first immigrants to this area.

The appearance of Murinae is usually documented by their rapid predominance in assemblages soon after their arrival (Dam *et al.* 2001). This is not the case in the Tuğlu section, where the presence of *Progonomys* in sample TU6/7 is followed by the absence of Murinae in sample TU19. Given that the stratigraphic sequence shows no evidence of overturning, folding or thrusting, the interpretation of the above finding remains uncertain. One of the possible explanations is that the fauna in sample TU19 was redeposited. However, the fauna preservation lacks evidence of long transport, thus not supporting this theory. On the other hand, some specimens are cracked, presumably due to pervasive microfracturing of sediments. Therefore, it seems more probable that the *Progonomys* specimens found in sample TU6/7 represent the very first

**Table 5**. Single-shell in situ $^{87}Sr/^{86}Sr$ isotopic ratios of adult *Cyprideis sublittoralis adentata* valves and Miliolidae tests as derived by LA-MC-ICPMS analysis.

| Sample | Single-shell $^{87}Sr/^{86}Sr$ | ±2σ | Shell type | Thickness [m] |
|---|---|---|---|---|
| TU42VF6 | 0.707677 | 0.000025 | adult ostracod valve | 24.35 |
| TU35V02 | 0.707596 | 0.000041 | adult ostracod valve | 20.45 |
| TU29V2 | 0.707596 | 0.000017 | adult ostracod valve | 17.05 |
| TU29V1r | 0.707249 | 0.000039 | adult ostracod valve | 17.05 |
| TU17V2 | 0.707213 | 0.000029 | adult ostracod valve | 8.40 |
| TU10V2 | 0.707129 | 0.000037 | adult ostracod valve | 4.50 |
| FO_TUHR28-03 | 0.707255 | 0.000027 | foraminifer test | 2.95 |
| TUHR20V2 | 0.707232 | 0.000029 | adult ostracod valve | 2.00 |
| FO_TUHR16c-08 | 0.707174 | 0.000035 | foraminifer test | 1.60 |
| TUHR12V2 | 0.707204 | 0.000014 | adult ostracod valve | 1.20 |

occurrence of Murinae in an area where they were still not common. The age interval represented between sample TU6/7 and sample TU19 was relatively short. Absence of *Progonomys* in the rodent assemblage from sample TU19 may therefore simply represent the scarcity of Murinae in that time and area, whether due to ecological factors or to the effect of sample size.

The ostracod assemblages from the Tuğlu section have yielded the characteristic Upper Miocene species *Cyprideis sublittoralis adentata*. This species is known from the Upper Miocene (Pannonian) in the Central Paratethys (Jiříček & Říha 1991), and from the Pannonian and Pontian of NW Turkey (Witt 2010). Although a wider stratigraphic range for this species cannot be ruled out, the occurrence of this species is most likely indicative for a Late Miocene age of the Tuğlu section.

All the recognised mollusc genera, except *Orientalina*, are recorded as Cenozoic fossils from Turkey and still live in this region (Taner 1994). From a chronostratigraphical point of view, only one taxon among the molluscs recorded in the Tuğlu Formation is indicative: the species *Melanopsis obesa*, which has been described from the Tortonian of the Hatay Basin (Erünal-Erentöz 1958). In areas other than Turkey, this species is recorded from the Late Miocene (early Pannonian, 11–10 Ma) of the Pannonian Basin, and from the Late Miocene (middle Pannonian, 10–9 Ma) of the Sava Basin (Croatia) (Harzhauser & Mandic 2008), pointing to a likely Tortonian age for the Tuğlu Formation.

The $\delta^{18}O$ values of the silty clay bulk samples translate to meteoric water oxygen isotope compositions ($\delta^{18}O_{mw}$) of –5 ± 2‰ (standard mean ocean water) under the assumption that carbonate precipitation took place in a temperature range of 13 ± 10 °C, using the calcite-water fractionation factors of Kim and O'Neil (1997). The reconstructed $\delta^{18}O_{mw}$ agrees well with the $\delta^{18}O_{mw}$ of the modern moisture controlling the precipitation budget of the margins of the CAP, but it is about 5 to 9.6‰ less negative than modern $\delta^{18}O_{mw}$ values of about –12‰ on the leeward sides of both the Pontide and Tauride Mountains. These first-order orographic units bordering the CAP exert a strong control on the fractionation of oxygen isotopes in precipitation (Schemmel *et al.* 2013). As will be shown below, evaporative enrichment, which could alternatively account for a positive shift in the reconstructed $\delta^{18}O_{mw}$ values, can be ruled out on the basis of the $\delta^{13}C$ vs. $\delta^{18}O$ correlation pattern in the whole-rock dataset (Figure 6B). This relationship provides evidence for an at least temporarily open hydrological regime of the Tuğlu palaeolake (i.e. low residence times) that does not favour evaporative enrichment of the heavy isotope $^{18}O$ in the water body.

Qualitatively, our new oxygen isotope data show that at the time the Tuğlu Formation was deposited, the topographic structure of Central Anatolia was markedly different from its present state, with no pronounced orographic barrier present for the moist air masses to cross. Such a barrier would have forced the advected moisture to preferentially lose the heavier $^{18}O$ isotope upon adiabatic cooling before reaching the plateau interior. The early uplift history of the margins of the CAP has been constrained using various records recently (Yildirim *et al.* 2011; Cosentino *et al.* 2012; Schildgen *et al.* 2012), with the uplift probably having commenced during the Late Tortonian. These major findings, when combined with the $\delta^{18}O$ values from the Tuğlu Formation, provide independent support for the biostratigraphic age constraints presented above and place a minimum limit on its age for the Late Tortonian.

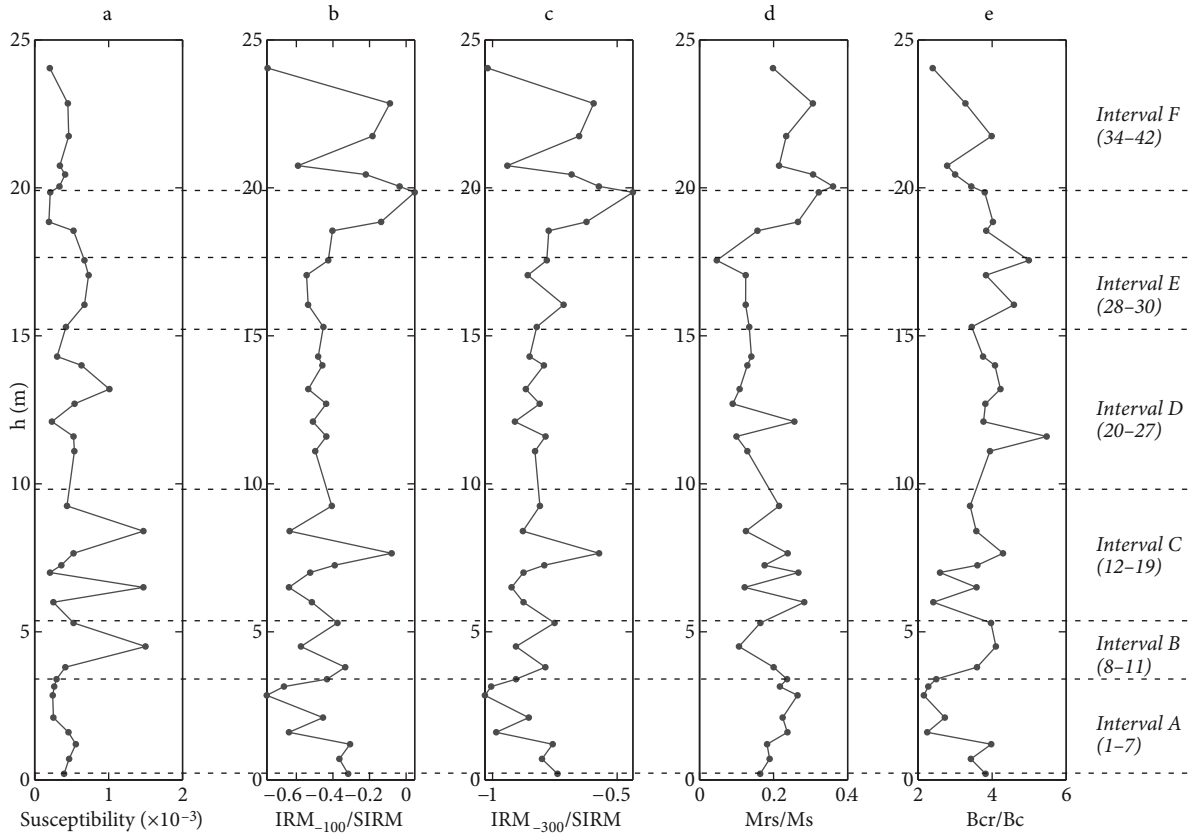


**Figure 8**. Environmental magnetism parameters measured on 41 samples from the Tuğlu section (from left to right): a) Susceptibility, b) $IRM_{-100}$/SIRM, c) $IRM_{-300}$/SIRM (S ratio; IRM acquired with a back field of 300 mT), d) Mrs/Ms (remanence ratio), e) Bcr/Bc (coercivity ratio).

### 5.2. Late Miocene palaeoenvironment

#### 5.2.1. Foraminifera and nannoplankton

The occurrence of foraminifera in a continental setting poses several questions both in terms of palaeogeography and palaeoecology. Morphological and taxonomical study of the foraminifera assemblages in the Tuğlu section points to several subsequent invasions of foraminifera into a saline water body. Aberrant coiling in the porcellaneous species can reflect changes in living conditions (Ponder 1974; Boltovskoy *et al*. 1991). Marine ingressions are difficult to explain from a geological point of view (Kaymakçı *et al*. 2010) because there has not been any evidence of any marine sediment in the basin since the late Oligocene. Moreover, only a very few species colonised the studied water body; planktonic, hyaline, and agglutinated taxa, which normally live in marginal marine conditions, were not recovered. An avian mediated foraminifera transport theory can be supported by the very low diversity of the assemblage, with a few species transported in a very juvenile state or as propagules of foraminifera (Scott *et al*. 2001; Sen Gupta 2002; Murray 2006). In fact, such a process has been commonly documented in a wide range of fresh water systems (e.g., Hayward & Hollis 1994). Some foraminifera are known to be able to survive the "drying-up" of ephemeral lakes (Cann & Deckker 1981), but porcellaneous taxa have not been studied in this context.

The reworked calcareous nannofossils may provide valuable clues about the stratigraphy of the sedimentary bedrocks exposed to erosion within the drainage area of the Tuğlu palaeolake. The most abundant forms are typical Palaeogene taxa, whereas the Cretaceous assemblage is quite scarce. However, reworking of nannofossils is a rather common phenomenon due to their hydraulic behaviour, and the composition of an allochthonous assemblage does not necessarily mirror the eroded stratigraphy adequately enough (Mikes *et al*. 2008).

#### 5.2.2. Ostracods

The ostracod assemblage consists of a mixture of euryhaline and freshwater species. Ostracods can be divided into 3 different ecological groups: truly brackish (*C. sublittoralis*), brackish to brackish tolerant (*Candona* (*Caspiocypris*) *postsarmatica*, *Ilyocypris* cf. *decipiens*, *Leucocythere camenice*, *Limnocytherina* sp.), and freshwater (*Z. membranae quadricella*, *Heterocypris* cf. *gregaria*,

**Table 6.** Biometrical parameters of the charophyte gyrogonites from sample TU21. Abbreviations: ISI = length/width ratio × 100; Conf. interv. = confidence interval; SD err. = standard deviation error; Var. $s^2$ = s/mean × 100 ; Var. index = variation index.

| | N | Min µm | Max µm | Mean µm | Conf. interv. µm | SD err. | Var $s^2$ | Var index % |
|---|---|---|---|---|---|---|---|---|
| *Nitellopsis merianii* | | | | | | | | |
| Length | 50 | 1000 | 1360 | 1186 | 1161–1211 | 91 | 8368 | 7.7 |
| Width | 50 | 760 | 1200 | 1012 | 983–1041 | 105 | 10,955 | 10.3 |
| ISI | 50 | 100 | 133 | 118 | 116–120 | 7 | 56 | 6.4 |
| *Lychnothamnus barbatus* | | | | | | | | |
| Length | 10 | 800 | 880 | 834 | 804–864 | 30 | 893 | 3.6 |
| Width | 10 | 640 | 740 | 698 | 681–715 | 27 | 751 | 3.9 |
| ISI | 10 | 108 | 128 | 120 | 116–124 | 6 | 38 | 5.1 |

*Cypria* sp.). *Cyprideis* species are generally characteristic of euryhaline environments, with an optimum in oligo- and mesohaline (brackish) waters. They may also live in waters with extremely high ion concentrations such as soda lakes or hyperhaline waters up to a salinity of 80‰ (Morkhoven 1963; Gross *et al.* 2008). *Cyprideis sublittoralis* has been reported from shallow, brackish water bodies (3‰–8‰) (Witt 2010). *Cyprideis torosa* Jones 1850, its recent counterpart, occurs in a wide range of salinities from almost freshwater to hyperhaline conditions, but its greatest abundance is observed at salinities of 2‰–16.5‰ in coastal ponds, lakes, lagoons, estuaries, fjords, deltas, and salt marshes (Meisch 2000: p. 463). In contrast, *Candona* (*Caspiocypris*) *postsarmatica* Krstić has been previously recovered in the Lower Pannonian of Carand (Pannonian Basin, Olteanu 2011), and from the *Congeria* Beds of the Pannonian Basin (Krstić 1972). *Candona* (*Caspiocypris*) *postsarmatica* is characteristic of the silty-clay facies of the lowermost Pannonian of the Pannonian basin (Olteanu 2011). *Zonocypris membranae quadricella* Stancheva 1966 occurs only in the upper part of the section (TU20–25), together with *Heterocypris* cf. *gregaria*, *Cypria* sp., *Leucocythere camenice*, and *Limnocytherina* sp. The most ancient record of *Z. membranae quadricella* is from the Serravalian of Morocco (Helmdach 1988 as *Z. maghrebinensis*). It also occurs in several brackish deposits from the Paratethys area (Stancheva 1966; Schneider in Suzin 1956; Mandelstam *et al.* 1962; Olteanu 1995; Krstić 2006) and is considered the only *Zonocypris* species adapted to brackish environments. *Zonocypris* species are known from the freshwater, slightly alkaline, shallow continental environment of Africa, tolerating water turbidity relatively well (Babinot 2003: p. 7). In the Tuğlu section, it indicates the only truly freshwater phase, as confirmed by the co-occurring taxa (charophyte species, molluscs *Lymnaea* and *Bithynia*). Freels (1980: p. 120) considers *H.* cf. *gregaria* a species characteristic of limnic and possibly also slightly brackish environments. In the Tuğlu section, it occurs in the freshwater phase as a dominant species, and it is therefore considered as indicative of freshwater conditions.

**5.2.3. Molluscs**

The lower part of the section (samples TU1–TU4) is characterised by fragmentary remains of freshwater gastropods, such as the opercula of *Bithynia* and *Melanopsis*. This environment may also not be suitable for shell preservation and points to the selective fluvial transport of the opercula into the palaeolake. This lower interval is followed by the establishment of a marsh environment (sample TU7), as shown by the occurrence of genera typical of well-vegetated calm waters, such as *Planorbarius* and *Lymnaea*.

In the middle part of the section (sample TU18), the occurrence of an oligotypic assemblage of terrestrial gastropods (Helicidae) points to a short-lived subaerial exposure. A shallow water lacustrine environment (sample TU23), with *Lymnaea* and *Bithynia* being the dominant gastropods, follows.

In the upper part, only scattered and transported fragmentary freshwater shells and opercula occur in a discontinuous manner for a long interval (10.5 to 17.0 m), indicating an environment not suitable for shell preservation. At the top (sample TU42), a rich assemblage of well-preserved freshwater gastropods, such as *Melanopsis obesa*, as well as disarticulated bivalves *Dreissena* sp. and *Potomida* sp., occur in a coarse matrix, pointing to the settlement of fluvial environment. All the mollusc taxa referred to in this layer, *Melanopsis*, *Dreissena*, and *Potomida*, prefer slow-flowing and fresh, oxygenated waters. *Melanopsis* can also tolerate low-oligohaline conditions (Lev *et al.* 2007).

Some thermophilous taxa were recorded from the Tuğlu Formation. Particularly *Melanopsis* and *Potomida* (often referred to as *Psilunio* in the literature, cf.

Machordom *et al*. 2006; Graf & Cummings 2007), having a wide distribution in the circum-Mediterranean and Middle East, point to warm conditions. Palaeotemperature derived from Late Cenozoic *Melanopsis* and *Potomida* shells from Turkey revealed a water temperature of 26.4 to 30.0 °C (Taner 1994).

**5.2.4. Charophyte gyrogonites**

All 3 charophyte taxa identified in the Tuğlu section were described earlier from the Cenozoic of Turkey (Mädler & Staesche 1979). All 3 species extend from the Oligocene to the Quaternary and are thus of little biostratigraphic value in the context of this study. *Nitellopsis merianii* (Table 6) was also recorded from the Messinian lacustrine series in the Velona Basin (Ghetti *et al*. 2002), and from the Ait Kandula palaeolake, Morocco (Soulié-Märsche *et al*. 2002). *Lychnothamnus barbatus* var. *antiquus* (Table 6) is known all over the Miocene epoch in southern France (Soulié-Märsche 1989) and extends through the Pliocene (Bhatia *et al*. 1998) up to recent times. *Chara molassica* appeared in the Oligocene and persisted up to the Early Quaternary (Mädler & Staesche 1979).

The assemblage of the 3 species, as well as each species separately, clearly refers to freshwater environments. By comparison with the single living species of the genus *Nitellopsis*, *N. obtusa*, the optimal environment for *Nitellopsis merianii* would correspond to permanent, relatively cold, alkaline lakes where the plants can reach a length of 2 m in the depth range of 4–12 m (Krause 1985; Soulié-Märsche *et al*. 2002). The modern *N. obtusa* supports mesotrophic waters but collapses at salinities >5‰ (Katsuhara & Tazawa 1986).

The rare extant species, *Lychnothamnus barbatus*, the modern analogue to var. *antiquus*, is characteristic for strictly oligotrophic freshwaters (Krause 1997) where it can reach a depth of 8 m in lakes in the Baltic area, e.g., in lakes in Lithuania (Balevicius 2001). No brackish water occurrence has been reported for *Lychnothamnus*.

Although most species of the genus *Chara* are freshwater macrophytes, salinity tolerance among the living *Chara* can reach 10‰–12‰. Due to this assemblage and to the high abundance of *Nitellopsis merianii*, with about 100 entire and about 200 broken gyrogonites isolated from sample TU21, the period covered by samples TU21–TU25 clearly corresponded to a freshwater episode in the evolution of the Tuğlu palaeoenvironment.

The sequence as exposed in the studied section was probably deposited in parts of a palaeolake where water depth did not exceed 10 m, because the extant *Nitellopsis* vegetation develops best from 2 m down to 12 m depths (Krause 1997). The latitudinal position of Tuğlu (at 40°25′23.8″3) implies a relatively high solar irradiance compared to localities in northern Europe and certainly favours the production of gyrogonites, as was observed in Holocene localities in North Africa (Kröpelin & Soulié-Märsche 1991; Soulié-Märsche 1993).

**5.2.5. Pollen**

The scarcity of pollen grains in the samples may be ascribable to a number of factors: high sedimentation rate, together with the pollen rain highly suspended in the matrix substance; subsequent destruction of pollen grains during fossilisation in aerated deposits; or low pollen production in the adjacent vegetation.

The biostratigraphic chart of Neogene strata in the Aegean region based on pollen data was first established by Benda *et al*. (1974) and by Benda and Muelenkamp (1990), who used spores and pollen assemblage biozones, including sporomorph associations, mainly for the biostratigraphic classification of the Late Oligocene to Pliocene strata. Akgün *et al*. (2007) studied, from the palynological point of view, selected continental Miocene sequences surrounding the Çorum area in the Çankırı Basin, while Kayseri and Akgün (2008) analysed the Serravalian-Tortonian sporomorph associations. The dominance of arctotertiary warm temperate geofloristic elements, together with the sporadic occurrence of palaeotropical ones in these studies, agree well with the climate interpretation based on our data. Both zonal and azonal forest associations accompanied the herb species located in the open vegetation units. Based on the pollen data studied herein, a subtropical–warm temperate climate with aridity and humidity oscillations prevailed in the Çankırı Basin. The herb and shrub dominance here reflects the landscape characteristics of the open grassland with local forests.

Mean annual temperature and mean annual precipitation in the Tuğlu section in the whole profile vary between 13.8 and 17 °C and 823 and 932 mm/year, respectively, which agrees well with the results of Kayseri and Akgün (2008) and Akkiraz *et al*. (2011).

**5.2.6. Other fossils**

The killifish *Aphanius* Nardo, 1827 is widely distributed in euryhaline and freshwater habitats of the Mediterranean Sea, Red Sea, Persian Gulf, and Arabian Sea, and also occurs in landlocked ponds and lakes, in small streams, and sometimes also in relatively large rivers, e.g., in Turkey and Iran (Villwock 1977; Wildekamp 1993; Coad 2000). *Aphanius* species typically thrive in environments that are not suitable for other groups of fish, and thus often lack direct competitors and major predators (Clavero *et al*. 2007).

The brachyuran genus *Potamon* lives exclusively in freshwater environments; thus, its presence in the fossil record indicates freshwater settings. The presence of fragmented cheliped and carapace remains indicate short transport prior to deposition (Klaus & Gross 2010). The occurrence of the genus *Potamon* is considered as an indicator of temperatures of the coldest month above 0 °C.

**5.2.7. Environmental magnetism**

The variations of the magnetic parameters shown in Figure 8 are interpreted in terms of their response to the environmental variations. Magnetic susceptibility is generally related to the variation of both paramagnetic and ferromagnetic minerals in the sediments, and in this case, since the variation of the magnetic susceptibility is not always related to the variation of the others magnetic mineral parameters, we suggest that there is a contribution of the paramagnetic minerals.

In the lower part of the section (interval A, Figure 8), the magnetic susceptibility records stable values whereas a variation of the others parameters is observed. This is related to a stable environment of the saline lake where these sediments are deposited, with absent or very low external inputs and a well-developed drainage pattern. The $IRM_{-100}$/SIRM and $IRM_{-300}$/SIRM are related to the presence of hard ferromagnetic minerals, such as hematite ($Fe_2O_3$). The decrease of these parameters in the interval A suggests that there were increasing anoxic conditions and a decrease of external input of hematite-bearing sediments (such as red beds).

In the central part of the section (intervals B, C, D, and E), a significant variation of all the magnetic parameters is recorded. The variation of magnetic susceptibility indicates variations in the terrigenous component and ferromagnetic minerals. Instead, variations in $IRM_{-100}$/SIRM and $IRM_{-300}$/SIRM suggest that hematite contribution to various degrees was probably related to the weathering of red beds in the surrounding area.

Mrs/Ms and Bcr/Bc parameters are closely linked to the magnetic mineral grain size as well, and so the lower peak could correspond to a lower energy of the saline lake and the higher values to an increase of the drainage energy.

In the upper part of the section (interval F), the environment changes in a more open environment with a well-developed drainage system. The susceptibility does not record any variation, not being sensitive enough; however, the other parameters show high variations related to the different grain sizes and the ferromagnetic input to the basin.

**5.2.8. Whole-rock and ostracod $\delta^{13}C$ and $\delta^{18}O$ values, and ostracod and foraminifer $^{87}Sr/^{86}Sr$ ratios: implications for palaeohydrology**

All $\delta^{18}O$ data are consistent with carbonate precipitation in a water body of meteoric origin and preclude any major marine influence. There is only a weak positive correlation between $\delta^{13}C$ and $\delta^{18}O$ values of the whole-rock samples ($r^2 \sim 0.5$). The oxygen isotopic ratios cluster in a relatively narrow range between –6‰ and – 4‰, consistent with stable lake water compositions, with the observed variations caused by minor fluctuations in temperature and/or in the composition of the net precipitation in the catchment throughout deposition (Leng & Marshall 2004). The carbon isotope data, in contrast, exhibit a larger variation from –13‰ to –5‰ (Figure 6B). This variation reflects short-term, high-frequency changes in the relative contribution of isotopically light carbon to the net carbon budget of the lake water, most likely resulting from changes in the runoff composition. Since carbon isotope composition of ground waters is influenced by vegetation density due to the preferential incorporation of $^{12}C$ from plant material, the observed variations in $\delta^{13}C$ are in agreement with a heterogeneous vegetation structure comprising open grassland and local forests as revealed by our palynological data. In addition, it cannot be excluded that a part of the heavy carbon isotope is linked to $CaCO_3$ dissolution in the inflow region, although it is difficult to assess the role of this process relative to the vegetation control.

Based on the little variation in the whole-rock $\delta^{18}O$ values, together with a wider range of $\delta^{13}C$ values as well as the weak correlation between them, we interpret the data as indicating an open water budget with low residence times in a relatively humid environment, with no indication for evaporative enrichment of $^{18}O$ (Talbot 1990; see also Cyr *et al*. 2005; Lüdecke *et al*. this volume). This interpretation is further supported by our palaeoenvironmental data, suggesting elevated rainfall values and a shallow depth for the Tuğlu palaeolake.

$\delta^{18}O$ values of adult *Cyprideis sublittoralis adentata* valves display a consistent offset of up to 2.5‰ relative to the whole-rock compositions. The magnitude of this offset is variable in intervals A and F, but relatively stable in intervals B and C. Whereas vital effects are likely important in shaping the observed isotopic offset, the variability also calls for additional environmental control superimposed on them (e.g., Janz & Vennemann 2005). To this end, we tentatively assign the nonvital component of the variable offsets to both seasonal effects (involving different lake-bottom water temperatures at the time of moulting) and changes in the likely ephemeral thermal stratification of the lake through time. Variations in *Cyprideis sublittoralis adentata* $\delta^{13}C$ values are somewhat lower than for $\delta^{18}O$ and agree fairly well with the $\delta^{13}C$ of the host sediment in any horizon of the section. Ostracod $\delta^{13}C$ values in a hydrologically open lake are controlled by the carbon isotope composition of the total dissolved inorganic carbon (TDIC), itself a function of TDIC composition of the riverine/groundwater influx, primary bioproductivity, and organic matter decay. Given the near-surface and bottom zones in the water column where fine-grained algal or inorganic carbonate and ostracod carbonate respectively precipitate, the good agreement between host sediment and ostracod $\delta^{13}C$ values strongly suggest that an effective vertical compositional homogenisation of the lake water went into completion.

Sr isotopic analysis of *Cyprideis sublittoralis adentata* and Miliolidae reveals rather low $^{87}Sr/^{86}Sr$ values for the water body of the Tuğlu palaeolake ranging from 0.707129 ± 0.000029 to 0.707677 ± 0.000025, significantly different from the global seawater values in the Neogene (0.708251 to 0.709068, Howarth & McArthur 1997; McArthur *et al.* 2001). In light of the high (up to hyperhaline, i.e. >40%) salinity conditions indicated by the microfaunal assemblage at the base of the section, as well as the lack of any potential long-term evaporative enrichment of ions as shown by the $\delta^{13}C$ and $\delta^{18}O$ data, the $^{87}Sr/^{86}Sr$ values indicate that the ultimate drivers of the high salinity were evaporitic bodies available to leaching by surface runoff and/or subsurface groundwater flows. A mild shift towards higher $^{87}Sr/^{86}Sr$ values at the base of interval E (Figure 7) indicates a slightly increased contribution from source lithologies rich in radiogenic Sr. This could possibly result from a change in the ratio of surface runoff to groundwater flux, a change in catchment configuration, or a combination thereof.

The $^{87}Sr/^{86}Sr$ values may provide valuable clues about the age of the evaporitic bodies using the global marine $^{87}Sr/^{86}Sr$ curve, and they are consistent with primary marine evaporitic deposition in pre-Late Miocene times. The measured $^{87}Sr/^{86}Sr$ ratios identify Permian, Jurassic, and/or Cretaceous marine evaporites as the most probable ultimate source for the Sr ions. The global marine $^{87}Sr/^{86}Sr$ values in these periods range from 0.706913 to 0.708166, 0.706847 to 0.707753, and 0.707173 to 0.707830, respectively (Howarth & McArthur 1997; McArthur *et al.* 2001). Any significant contribution of Sr released from carbonate and ophiolitic lithologies can likely be ruled out on the grounds of mass-balance considerations and the slow rate at which they release Sr into groundwaters as compared to the highly soluble evaporites. In fact, in the Çankırı Basin and its surroundings, there are a number of evaporitic bodies, which could potentially contribute to the salinity budget of the Tuğlu palaeolake, such as Cretaceous to Oligocene gypsum layers and domes in the Tuz Gölü area, Mihallıççık-Beypazarı, Çankırı-Çorum, and Sivas basins (Tekin 2001; Çelmen & Çelik 2009; Kaymakçı *et al.* 2010).

However, dissolution and reprecipitation of evaporites occurred in the Early Tertiary in an overall closed endorheic setting, which likely resulted in the deposition of evaporitic sequences with a Sr isotopic signature inherited from their marine precursor(s). For example, a salt sequence of over 2000 m thick of uncertain Early Tertiary (Middle Eocene to Oligocene?) age exists in the subsurface of the Çankiri Basin as revealed by the Sağpazarı-1 well (e.g., Grove *et al.* 2004). $^{87}Sr/^{86}Sr$ ratios from 5 evaporite samples range from 0.707392 ± 11 to 0.707962 ± 21 (M.R. Palmer *et al.* 2004). These values are rather comparable to those reconstructed for the Tuğlu water body. Likely, the Late Miocene extension of the Anatolian plate (Yildirim *et al.* 2011) together with an overall humid climate as demonstrated herein favoured evaporitic flow, the formation of subsurface meteoric water pathways, and thus enhanced evaporitic leaching.

The faunal assemblages indicate temporary oscillations of the water levels and variations in salinity, which could be linked to climatic events (e.g., increase in precipitation, drought periods).

### 5.2.9. Whole-rock total organic carbon content

The TOC was used here as a palaeoproductivity indicator (Meyers 1997). In general, the TOC values are relatively

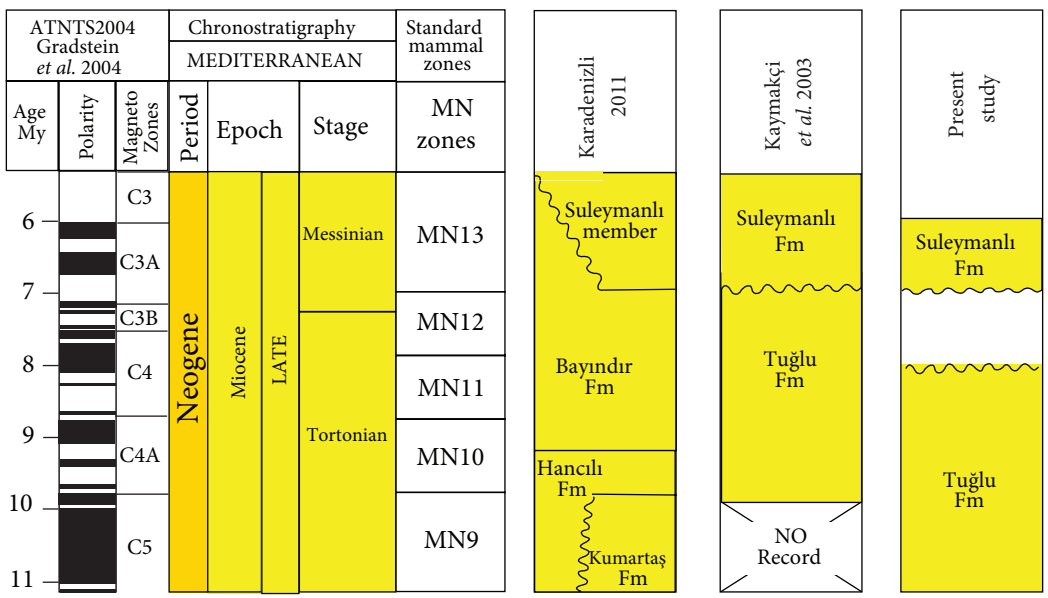


**Figure 9**. Different stratigraphic interpretation of the Late Miocene deposits in the N Çankırı-Çorum Basin.

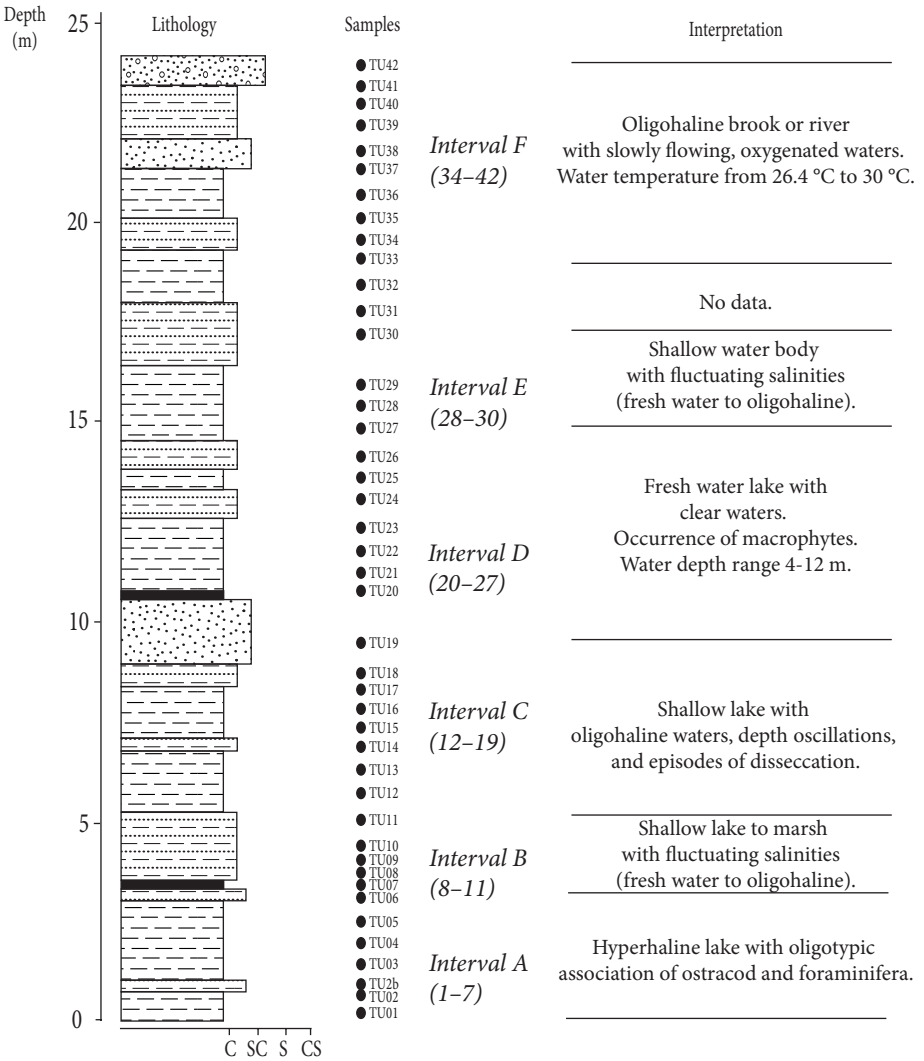


**Figure 10.** Palaeoenvironmental interpretation of the Tuğlu section: the intervals were identified combining all the palaeontological proxies.

low, but postdepositional processes might cause this. In the lower part, the TOC values are relatively high with a decreasing trend up-section, probably due to increasing salinity of the lake, which likely corresponds to higher organic productivity during the sedimentation. The stable isotope and some of the palaeontological data indicate an open hydrological environment, which translates to a rapid replenishment of the water mass. The overall low TOC values are probably a result of relatively fast sedimentation (in agreement with elevated rainfall values as derived from the pollen data), with the terrigenous clay input overwhelming the amount of organic matter available for burial. In addition, episodic mild oxidation directly at the lake bottom, as suggested by the environmental magnetic parameters, might have led to a partial breakdown of the organic matter prior to burial. There is, however, no clear-cut correlation between TOC and carbonate concentration in the sediments. During the early Late Miocene, absolute mean annual precipitation in central Europe underwent a drastic increase, from about 400 mm/year to 1200 mm/year (Böhme *et al*. 2008). The interactions of changing rainfall patterns in central Europe, associated changes in North Atlantic moisture transport trajectories, and cross-Mediterranean moisture transport in the Miocene are currently only poorly constrained. Given that North Atlantic circulation patterns ultimately determine moisture transport to central and eastern Europe, it is conceivable that teleconnections exist that transport these changes in rainfall to the Tuğlu region (Micheels *et al*. 2011).

## 6. Conclusions

Our results refine the stratigraphical position and the palaeoenvironmental interpretation of the Tuğlu Formation in the Çankırı Basin and contribute to better understanding of the timing of the uplift of the CAP during the Late Miocene.

1) Stratigraphy of Tuğlu Formation: The new biostratigraphic data point to the lower MN9 biozone (early Tortonian age) for the onset of the Tuğlu Formation. With respect to the stratigraphic schemes proposed by Kaymakçı (2000) and by Karadenizli (2011), our results imply that the deposition of the Tuğlu Formation started earlier than reported before (Figure 9). The palaeomagnetic data indicate that all the samples have a normal polarity. This allows us to constrain the deposition of the Tuğlu section to one of the normal polarity events at the base of the MN9 zone (Figure 9).

2) Palaeoenvironment (Figure 10): Charophytes, molluscs, crustaceans, foraminifera, and fish have yielded freshwater and brackish forms as well as marine–euryhaline taxa. Accordingly, the Tuğlu Formation may be interpreted as the deposit of a shallow saline lake, which evolved to a lake and subsequently to a low-energy fluvial environment. The occurrence of marine–euryhaline foraminifera at the base of the section and their isotopic signatures cannot be explained with any marine connection via ancient seaways. In contrast, their occurrence is most likely accounted for by passive transport into an environment with suitable salinity. The salinity budget in the basin was strongly influenced by subsurface leaching of pre-Miocene evaporites in a dominantly extensional tectonic regime and under relatively humid climatic conditions. Reconstructed mean annual temperature and mean annual precipitation in the Tuğlu section vary between 13.8 and 17 °C and 823 and 932 mm/year, respectively. These conditions gave rise to enhanced groundwater flow and high salinity in the Tuğlu palaeolake, as confirmed by all the abiotic parameters analysed. The magnetic parameters $IRM_{-100}$/SIRM, $IRM_{-300}$/SIRM, Mrs/Ms, and Bcr/Bc display remarkable oscillations in correspondence to intervals C, D, and F (Figures 8 and 10).

3) Relation between the Tuğlu Formation and the surface uplift history of Central Anatolia: Stable oxygen isotope records from the Tuğlu section, when taken together with published data on the timing of uplift of the southern margin of the Central Anatolian Plateau, as well as on modern meteoric water $\delta^{18}O$ values, point to reconstructed meteoric water $\delta^{18}O$ values that are most consistent with an essentially flat topography with no prominent mountain belts developed yet at the plateau margins. The palaeontological indications point to an age younger than 11.1 Ma (base of MN9) for the onset of the deposition of the Tuğlu Formation. Literature data (Kaymakçı 2000; Karadenizli 2011) broaden the depositional timing of the Tuğlu Formation until MN11 (around 8 Ma). We can assume that at least until the end of the deposition of the Tuğlu Formation, the north-central part of the CAP, where the Çankırı Basin is located, was not yet uplifted. The post-8 Ma age for the start of surface uplift of this area is in good agreement with the timing of uplift recorded in the southern margin of the CAP by Cosentino *et al*. (2012).

**Acknowledgements**

This research is part of the Vertical Anatolian Movements Project (VAMP), funded by the TOPO-EUROPE initiative of the European Science Foundation, with contributions by the Istituto di Geologia Ambientale e Geoingegneria (IGAG-CNR com. TA.P05.009, mod. TA.P05.009.003), the Slovak Research and Development Agency (SRDA-project number ESF-EC-009-07), the Scientific and Technological Research Council of Turkey (TÜBİTAK Grant No. 107Y333 to B.R.), the German Science Foundation (grant DFG MU 2845/1-1 to A.M.), and the LOEWE funding program of Hesse's Ministry of Higher Education, Research, and the Arts.

Our most sincere gratitude goes to Nuretdin Kaymakçı for sharing his knowledge on the regional geology and for his continued support. Barbara Zahradníková, Eva Halásová, Matúš Hyžný, Katarína Šarinová, and Torsten Utescher are thanked for the identification of the otoliths, nannofossils, freshwater crab, major elements interpretation, and the quantification of palaeoclimate data (CA), respectively.

Ažbeta Svitáčová from the IR laboratory of GI SAS (Slovakia) is thanked for performing the TOC analysis. We are thankful to Hans de Bruijn from University Utrecht, the Netherlands, for the material provided and the helpful comments. Special thanks go to Axel Gerdes for his essential help with the Sr isotope analyses, as well as to Christiane Wenske, Hannover, and Ulrich Treffert, Frankfurt am Main, for laboratory assistance.

The LOWESS fit of the global Sr record (version IV: 08/04) was kindly provided by John McArthur. We thank Halim Mutlu, Pere Anadón, and László Kocsis for their constructive comments and suggestions, which greatly improved the manuscript.

## References

Aguilar, J.P., Calvet, M. & Michaux, J. 1991. Présence de Progonomys (Muridae, Rodentia, Mammalia) dans une association de rongeurs de la fin du Miocène moyen (Castelnou 1B; Pyrénées-orientales, France). *Geobios* **24**, 504–508.

Akgün, F., Kayseri, M.S. & Akkiraz, M.S. 2007. Paleoclimatic evolution and vegetational changes during the Late Oligocene–Miocene period in western and central Anatolia (Turkey). *Palaeogeography, Palaeoclimatology, Palaeoecology* **253**, 56–106.

Akkiraz, M.S., Akgün, F., Utescher, T., Bruch, A.A. & Mosbrugger, V. 2011. Precipitation gradients during the Miocene in Western and Central Turkey as quantified from pollen data. *Palaeogeography, Palaeoclimatology, Palaeoecology* **304**, 276–290.

Alberdi, M.T., López, N., Morales, J., Sesé, C. & Soria, D. 1981. Bioestratigrafía y biogeografía de la fauna de Mamíferos de Los Valles de Fuentidueña (Segovia). *Estudios Geologicos* **37**, 503–511.

Armstrong-Altrin, J. & Verma, S., 2005. Critical evaluation of six tectonic setting discrimination diagrams using geochemical data of Neogene sediments from known tectonic settings. *Sedimentary Geology* **177**, 115–129.

Babinot, J.F. 2003. *Zonocypris digitalis* (Ostracoda, Crustacea), a new species from the Fuvelian (non marine Campanian) of Provence (south-east France). *Revue de micropaléontologie* **46**, 3–9.

Balevicius, A. 2001. Distribution of *Lychnothamnus barbatus* community in Lithuania. *Biologija* **2**, 70–73.

Benda, L., Innocenti, F., Mazzuoli, R., Radiacati, F. & Steffens P. 1974. Stratigraphic and radiometric data of the Neogene in northwest Turkey (Cenozoic and Lignites in Turkey, 16). *Zeitschrift der Deutschen Geologischen Gesellschaft* **125**, 183–193.

Benda, L. & Meulenkamp, J.E. 1990. Biostratigraphic correlations in the eastern Mediterranean Neogene 9. Sporomorph associations and event stratigraphy of the Eastern Mediterranean Neogene. *Newsletter Stratigraphy* **23**, 1–10.

Bhatia, S.B., Soulié-Märsche, I. & Gemayel, P. 1998. Late Pliocene and Early Pleistocene charophyte floras of the Hirpur Formation, Karewa Group, Kashmir, India. *N. Jb. Geol. Paläontol., Abh.* **210**, 185–209.

Birgili, Ş., Yoldaş, R. & Ünalan, G. 1975. *Çankırı-Çorum havzasının jeolojisi ve petrololanakları*. MTA Report No: 5621, Ankara.

Böhme, M., Ilg, A. & Winklhofer M. 2008. Late Miocene "washhouse" climate in Europe. *Earth and Planetary Science Letters* **275**, 393–401.

Boltovskoy, E., Scott D.B. & Medioli F.S. 1991. Morphological variations of benthic foraminiferal tests in response to changes in ecological parameters: a review. *Journal of Paleontology* **65**, 175–185.

Boomer, I., Horne D.J. & Slipper I.J. 2003. The use of ostracods in palaeoenvironmental studies, or what can you do with an ostracod shell? *In:* Park, L.E. & Smith, A.J. (eds) *Bridging the Gap. Trends in the Ostracode Biological and Geological Sciences*, Paleontological Society Paper **9**, 153–180.

Cann, J.H. & De Deckker, P. 1981. Fossil Quaternary and living foraminifera from athalassic (non-marine) saline lakes, southern Australia. *Journal of Paleontology* **55**, 660–670.

Çelmen, O. & Çelik, M. 2009. Hydrochemistry and environmental isotope study of the geothermal water around Beypazari granitoids. *Environmental Geology* **58**, 1689–1701.

Clavero, M., Blanco-Garrido, F. & Prenda, J. 2007. Population and microhabitat effects of interspecific interactions on the endangered Andalusian toothcarp (*Aphanius baeticus*). *Environmental Biology of Fishes* **78**, 173–182.

Coad, B.W. 2000. Distribution of *Aphanius* species in Iran. *Journal of the American Killifish Association* **33**, 183–191.

Cosentino, D., Schildgen, T.F., Cipollari, P., Faranda, C., Gliozzi, E., Hudáčková, N., Lucifora, S. & Strecker, M.R. 2012. Late Miocene surface uplift of the southern margin of the Central Anatolian Plateau, Central Taurides, Turkey. *GSA Bulletin* **124**, 133–145.

Cyr, A.J., Currie, B.S. & Rowley, D.B. 2005. Geochemical evolution of Fenghuoshan Group lacustrine carbonates, North-Central Tibet: implications for the paleoaltimetry of the Eocene Tibetan Plateau. *The Journal of Geology* **113**, 517–533.

Dam, J.A. van, Alcalá, L., Alonso Zarza, A.M., Calvo, J.P., Garcés, M. & Krijgsman, W. 2001. The Upper Miocene mammal record from the Teruel-Alfambra region (Spain): the MN system and continental Stage/Age concepts discussed. *Journal of Vertebrate Paleontology* **21**, 367–385.

Day, R., Fuller, M. & Schmidt, V.A. 1977. Hysteresis properties of titanomagnetites: grain-size and compositional dependence. *Physics of The Earth and Planetary Interiors* **13**, 260–267.

Dunlop, D.J. 2002. Theory and application of the Day plot (Mrs/Ms versus Hcr/Hc) 1. Theoretical curves and tests using titanomagnetite data. *Journal of Geophysical Research* **107**, 1–22.

Dunlop, D.J. & Carter-Stiglitz, B. 2006. Day plots of mixtures of superparamagnetic, single-domain, pseudosingle-domain, and multidomain magnetites. *Journal of Geophysical Research* **111**, 1–10.

Erdtman, G. 1943. *An Introduction to Pollen Analysis*. Chronica Botanica, Waltham, MA, USA.

Erünal-Erentöz, L. 1958. Mollusques du Néogène des Bassins de Karaman, Adana et Hatay (Turquie). *Publications de l'Institut d'Études et de Recherches Minières de Turquie, sér. C* **4**, 1–232.

Fejfar, O., Heinrich, W.D., Kordos, L. & Maul, L.C. 2011. Microtoid cricetids and the early history of arvicolids (Mammalia, Rodentia). *Palaeontologia Electronica* **14**, 38.

Fortelius, M., Werdelin, L., Andrews, P., Bernor, R.L., Gentry, A., Humphrey, L., Mittmann, W. & Viranta, S. 1996. Provinciality, diversity, turnover and paleoecology in land mammal faunas of the later Miocene of western Eurasia *In:* Bernor, R., Fahlbusch, V. & Mittmann W. (eds), *The Evolution of Western Eurasian Neogene Mammal Faunas*. Columbia University Press, New York, 414–448.

Freels, D. 1980. Limnische Ostrakoden aus Jungtertiär und Quartär der Türkei. *Geologisches Jahrbuch B* 39, 3–169.

Gannser, A. 1974. The ophiolitic mélange, a world-wide problem on Tethyan examples. *Eclogae Geologicae Helvetiae* **67/3**, 479–507.

Ghetti, P., Anadón, P., Bertini, A., Esu, D., Gliozzi, E., Rook, L. & Soulié-Märsche I. 2002. The Early Messinian Velona Basin (Siena, Central Italy): palaeoenvironmental and palaeobiogeographical reconstructions. *Palaeogeography, Palaeoclimatology, Palaeoecology* **292**, 5, 1–33.

Graf, D.L. & Cummings, K.S. 2007. Review of the systematics and global diversity of freshwater mussel species (Bivalvia: Unionoida). *Journal of Molluscan Studies* **73**, 291–314.

Grambast, N. & Soulié-Märsche, I. 1972. Sur l'ancienneté et la diversification des *Nitellopsis* (Charophytes). *Paléobiologie Continentale* **III** (3), 1–14.

Gross, M., Minati, K., Danielopol, D. & Piller, W. 2008. Environmental changes and diversification of *Cyprideis* in the Late Miocene of the Styrian Basin (Lake Pannon, Austria). *Senckenbergiana lethaea* **88**, 161–181.

Grove, K.W., Silverman, M.R., Rasmussen, D.R., Penfield, G.T., Gurnert, W.R. & Grateral, V. 2004. Geophysical evaluation and exploration potential of the Haymana-Polatli and Cankiri Basins, Central Anatolia, Turkey. AAPG Search and Discovery Article #90024©2000, AAPG Regional International Conference, İstanbul, Turkey.

Harzhauser, M. & Mandic, O. 2008. Neogene lake systems of Central and South-Eastern Europe: faunal diversity, gradients and interrelations. *Palaeogeography, Palaeoclimatology, Palaeoecology* **260**, 417–434.

Hayward, B.W. & Hollis, C.J. 1994. Brackish foraminifera in New Zealand: a taxonomic and ecologic review. *Micropaleontology* **40**: 185–222.

Helmdach, F.F. 1988. The ostracode fauna of the Ait Kandoula region, systematic description. *In:* Jacobshagen, V.H. (ed), *The Atlas System of Morocco*. Springer-Verlag, Berlin, 405–432.

Hohenegger, J. 2005. Estimation of environmental paleogradient values based on presence/absence data: a case study using benthic foraminifera for paleodepth estimation. *Palaeogeography, Palaeoclimatology, Palaeoecology* **217**, 115–130.

Howarth, R.J. & McArthur, J.M. 1997. Statistics for strontium isotope stratigraphy: A robust LOWESS fit to the marine Sr-isotope curve for 0 to 206 Ma, with look-up table for the derivation of numerical age. *Journal of Geology* **105**, 441–456.

McArthur, J.M., Howarth, R.J. & Bailey, T.R., 2001. Strontium isotope stratigraphy: LOWESS Version 3: Best-fit line to the marine Sr-isotope curve for 0 to 509 Ma and accompanying look-up table for deriving numerical age. *Journal of Geology* **109**, 155–169.

Janz, H. & Vennemann, T. 2005. Isotopic composition (O, C, Sr, and Nd) and trace element ratios (Sr/Ca, Mg/Ca) of Miocene marine and brackish ostracods from North Alpine Foreland deposits (Germany and Austria) as indicators for palaeoclimate. *Palaeogeography, Palaeoclimatology, Palaeoecology* **225**, 216–247.

Jin, Z., Bickle, M., Chapman, H., Yu, J., Greaves, M., Wang, S. & Chen, S. 2006. An experimental evaluation of cleaning methods for fossil ostracod Mg/Ca and Sr/Ca determination. *Journal of Paleolimnology* **36**, 211–128.

Jiříček, R. & Říha, J. 1991. Correlation of ostracod zones in the Paratethys and Tethys. *Saito Ho-on Kai Special Publications (Proceedings of Shallow Tethys)* **3**, 435–457.

Kappelman, J., Duncan, A., Feshea, M., Lunkka, J.P., Ekart, D., Mcdowell, F., Ryan, T. & Swisher C.C. 3rd. 2003. Chronology of the Sinap Formation. In: Fortelius, M., Kappelman, J., Sen, S. & Bernor, R.L. (eds), *Geology and Palaeontology of the Miocene Sinap Formation, Turkey*. Columbia University Press, New York, 41–66.

Karadenizli, L. 2011. Oligocene to Pliocene palaeogeographic evolution of the Çankırı-Çorum Basin, central Anatolia, Turkey. *Sedimentary Geology* **237**, 1–29.

Katsuhara, M. & Tazawa, M. 1986. Salt tolerance in *Nitellopsis obtusa*. *Protoplasma* **135**, 155–161.

Kaymakci, N. 2000. Tectono-stratigraphical Evolution of the Çankırı Basin (Central Anatolia, Turkey). PhD Thesis, Universiteit Utrecht, Utrecht.

Kaymakçı, N., Özmutlu, Ş., Van Dijk, P.M. & Özçelik, Y. 2010. Surface and subsurface characteristics of the Çankırı Basin (Central Anatolia, Turkey): integration of remote sensing, seismic interpretation and gravity. *Turkish Journal of Earth Sciences* **19**, 79–100.

Kaymakçi, N., White, S.H. & van Dijk, P.M. 2000. Paleostress inversion in a multiphase deformed area: kinematic and structural evolution of the Çankırı basin (central Turkey), Part 1 – northern area. *In:* Bozkurt, E., Winchester, J.A. & Piper, J.D.A. (eds), *Tectonics and Magmatism in Turkey and the Surrounding Area*. Geological Society, London, Special Publications **173**, 295–323.

Kaymakçi, N., White, S.H. & van Dijk, P.M. 2003. Kinematic and structural development of the Çankırı Basin (Central Anatolia, Turkey). A paleostress inversion study. *Tectonophysics* **364**, 85–113.

Kayseri, M.S & Akgün, F. 2008. Palynostratigraphic, palaeovegetational and palaeoclimatic investigations on the Miocene deposits in Central Anatolia (Çorum Region and Sivas Basin). *Turkish Journal of Earth Sciences* **17**, 361–403.

Kim, S.T. & O'Neil, J.R. 1997. Equilibrium and nonequilibrium oxygen isotope effects in synthetic carbonates. *Geochimica et Cosmochimica Acta* **61**, 3461–3475.

Kissel, C., Laj, C., Poisson, A. & Görür, N. 2003. Paleomagnetic reconstruction of the Cenozoic evolution of the Eastern Mediterranean. *Tectonophysics* **362**, 199–217.

Klaus, S. & Gross, M. 2010. Synopsis of the fossil freshwater crabs of Europe (Brachyura: Potamoidea: Potamidae). *Neues Jahrbuch für Geologie und Paläontologie, Abh.* **256**, 39–59.

Kovar-Eder, J., Jechorek, H., Kvaček, Z. & Parashiv, V. 2008. The integrated plant record: an essential tool for reconstructing Neogene zonal vegetation in Europe. *Palaios* **23**, 97–11.

Krause, W. 1985. Über die Standortsansprüche und das Ausbreitungsverhalten der Stern-Armleuchter-alge *Nitellopsis obtusa* (Desvaux) J. Groves. *Carolinea* **42**, 31–42.

Krause, W. 1997. *Charales (Charophyceae). Süsswasserflora von Mitteleuropa. Band 18.* Gustav Fischer Verlag, Jena, 1–202.

Krstić, N. 1972. Genus *Candona* (Ostracoda) from Congeria Beds of Southern Pannonian Basin, (Summary). *Monographs Vo. CDL, The Section of Natural and Mathematical Sciences* **39**, 1–200 [in Serbian with extended English summary].

Krstić, N. 2006. Pliocene ostracodes of the Paludinian Beds in the Pannonian Plain, Serbian part. *Herald of the Natural History Museum*, 1–409.

Kröpelin, S. & Soulié-Märsche, I. 1991. Charophyte remains from Wadi Howar as evidence for deep mid-Holocene freshwater lakes in Eastern Sahara (NW Sudan). *Quaternary Research* **36**, 210–223.

Le Maitre, R.W. 1976. The chemical variability of some common igneous rocks. *Journal of Petrology* **17**, 589–637.

Leng, M.J. & Marshall, J.D. 2004. Palaeoclimate interpretation of stable isotope data from lake sediment archives. *Quaternary Science Reviews* **23**, 811–831.

Lev, L., Boaretto, E., Heller, J., Marco, S. & Stein, M. 2007. The feasibility of using *Melanopsis* shells as radiocarbon chronometers, Lake Kinneret, Israel. *Radiocarbon* **49**, 1003–1015.

Lüdecke, T., Mikes, T., Rojay, B., Cosca, M.A. & Mulch, A. Dynamic Middle Cenozoic paleoenvironments of the Central Anatolian Plateau: insights from stable isotope records and tuff geochronology of continental deposits. *Turkish Journal of Earth Sciences*, this volume.

Machordom, A., Araujo, R., Nagel, K.O., Reis, J. & Toledo, C. 2006. A preliminary phylogeny of the European Unionoidea. *In:* Malchus, N. & Pons, J.M. (eds), *International Congress on Bivalves*. Organisms Diversity and Evolution **6**, Electr. Suppl. **16**, 1–53.

Mädler, K. & Staesche, U. 1979. Fossile Charophyten aus dem Känozoikum (Tertiär und Quartär) der Türkei. *Geologisches Jahrbuch* **B33**, 81–157.

Mai, D.H. 1991. Palaeofloristic changes in Europe and the confirmation of the Arctotertiary-Palaeotropical geofloral concept. *Review of Paleobotany and Palynology* **68**, 29–36.

Mandelstam, M.I., Markova, L.P., Rozyeva, T.R. & Stepanaitys, N.E. 1962. *Ostracoda of the Pliocene and Post-Pliocene Deposits of Turkmenistan*. Turkmenistan Geological Institute, Ashkhabad, 1–288 [in Russian].

Meisch, C. 2000. Freshwater Ostracoda of Western and Central Europe. *In:* Schwoerbel, J. & Zwick, P. (eds), *Süßwasserfauna von Mitteleuropa* **8**. Spektrum Akademischer Verlag, Heidelberg-Berlin, 1–522.

Meriç, E., Avşar, N., Görmüş, M., & Bergin, F. 2004. Twin and triplet forms of recent benthic foraminifera from the eastern Aegean Sea, Turkish coast. *Micropaleontology* **50**, 297–300.

Meyers, P.A. 1997. Organic geochemical proxies of paleoceanographic, paleolimnologic and paleoclimatic processes. *Organic Geochemistry* **27**, 213–250.

Micheels, A., Bruch, A.A., Eronen J., Fortelius, M., Harzhauser, M., Utescher, T. & Mosbrugger, V. 2011. Analysis of the heat transport mechanism from a Late Miocene model experiment with a fully-coupled atmosphere-ocean general circulation model. *Palaeogeography, Palaeoclimatology, Palaeoecology* **304**, 337–350.

Mikes, T., Dunkl, I., von Eynatten, H., Báldi-Beke, M. & Kázmér, M. 2008. Calcareous nannofossil age constraints on Miocene flysch sedimentation of the Outer Dinarides (Slovenia, Croatia, Bosnia-Herzogovina, Montenegro). *In:* Siegesmund, S., Fügenschuh, B. & Froitzheim, N. (eds), *Tectonic Aspects of the Alpine-Dinaride-Carpathian System*, Geological Society of London, Special Publication **298**, 335–363.

Mikes, T., Gerdes, A., Hudáčková, N. & Mulch, A. 2011. $^{87}Sr/^{86}Sr$ isotope ratios in single benthic foraminifera by LA-MCICPMS. *Mineralogical Magazine, Goldschmidt Conference Abstracts* **75**, 1468.

Morkhoven, F.P.C.M. van 1963. *Post-Palaeozoic Ostracoda. Vol. II, Generic Descriptions*. Elsevier, Amsterdam, 1–478.

Mosbrugger, V. & Utescher, T. 1997. The coexistence approach — a method for quantitative reconstructions of Tertiary terrestrial paleoclimate data using the plant fossils. *Palaeogeography, Palaeoclimatology, Palaeoecology* **134**, 61–86.

Murray, J.W. 1973. *Distribution and Ecology of Living Benthic Foraminiferids*. Heinemann, London, 1–288.

Murray, J.W. 2006. *Ecology and Applications of Benthic Foraminifera*. Cambridge University Press, Cambridge, 1–426.

Nardo, J.D. 1827. Prodromus observationum et disquisitionum ichthyologiae Adriaticae. *Giornale di Fisica, Chimica, Storia naturale, Medicine ed Arti. Pavia, Italy* **2**, 22–40.

Nesbitt, H.W. & Young, G.M., 1982. Early Proterozoic climates and plate motions inferred from major element chemistry of lutites. *Nature* **299**, 715–717.

Nesbitt, H.W. & Young, G.M. 1984. Prediction of some weathering trends of plutonic and volkanic rocks based on thermodynamic and kinetic considerations, *Geochimica et Cosmochimica Acta* **48**, 1523–1534.

Olteanu, R. 1995. Dacian ostracodes. *In:* Marinescu, F. & Papaianopol, I. (eds), *Chronostratigraphie und Neostratotypen. Neogene der Zentrale Paratethys, Bd. IX*. Dacien, Editura Academiei Române, Bucharest, 268–385.

Olteanu, R. 2011. Atlas of the Pannonian and Pontian ostracods from the Eastern area of the Pannonian Basin. *Geo-Eco-Marina* **17**, 135–177.

Palmer, C.A., Tuncalı, E., Dennen, K.O., Coburn, T.C. & Finkelman, R.B. 2004. Characterization of Turkish coals: a nationwide perspective. *International Journal of Coal Geology* **60**, 85–115.

Palmer, M.R. Helvaci, C. & Fallick A.E. 2004. Sulphur, sulphate and strontium isotope composition of Cenozoic Turkish evaporites. *Chemical Geology* **209**, 341–356.

Ponder, R.W. & Glendinning, I.G. 1974. The magnesium content of some miliolacean foraminifera in relation to their ecology and classification. *Palaeogeography, Palaeoclimatology, Palaeoecology* **15**, 29–32.

Rochette, P. 1987. Magnetic susceptibility of the rock matrix related to magnetic fabric studies. *Journal of Structural Geology* 9, 1015-1020.

Rojay, B. 2012. Tectonic evolution of the Cretaceous Ankara Ophiolitic Mélange during the Late Cretaceous to pre-Miocene interval in Central Anatolia, Turkey. *Journal of Geodynamics* **59**, 10.1016/j.jog.2012.06.006.

Rojay, B., Altıner, D., Özkan Altıner, S., Önen, P., James, S. & Thirwall, M. 2004. Geodynamic significance of the Cretaceous pillow basalts from North Anatolian Ophiolitic Mélange Belt (Central Anatolia, Turkey): geochemical and paleontological constrains. *Geodinamica Acta* **17/5**, 349–361.

Rotstein, Y. 1984. Counterclockwise rotation of the Anatolian Block. *Tectonophysics* **108**, 71–91.

Sagnotti, L. 1998. Magnetic fabric of clay sediments from the external northern Apennines (Italy). *Physics of the Earth and Planetary Interiors* **105**, 73–93.

Schemmel, F., Mikes, T., Rojay, B. & Mulch, A; (2013). Towards stable isotope paleoaltimetry of Central Anatolia: A perspective from modern meteoric waters. *American Journal of Science* **313,** 61–80.

Schildgen, T.F., Cosentino, D., Bookhagen, B., Niedermann, S., Yildirim, C., Echtler, H.P., Wittmann, H. & Strecker, M.R. 2012. Multi-phase uplift of the southern margin of the Central Anatolian plateau: a record of tectonic and upper mantle processes. *Earth and Planetary Science Letters* **317–318**, 85–95.

Scott, D.B., Medioli F.S. & Schafer, C.T., 2001. *Monitoring in Coastal Environments Using Foraminifera and Thecamoebian***.** Cambridge University Press, Cambridge, 1–177.

Sen, S. 2003. Muridae and Gerbillidae (Rodentia). *In:* Fortelius, M., Kappelman, J., Sen, S. & Bernor, R.L. (eds), *Geology and Paleontology of the Miocene Sinap Formation, Turkey*. Columbia University Press, New York, 125–140.

Şengör, A.M.C. & Yılmaz, Y. 1981. Tethyan evolution of Turkey: a plate tectonic approach. *Tectonophysics* **75**, 181–241.

Sen Gupta, B.K. 2002. *Modern Foraminifera*. Kluwer Academic, Dordrecht, 1–384.

Sgarrella, A.F. & Moncharmont-Zei, M. 1993. Benthic foraminifera in the Gulf of Naples (Italy): systematic and autoecology. *Bollettino della Societa Paleontologica Italiana* **32**, 145–264.

Soulié-Märsche, I. 1989. *Etude comparée de gyrogonites de Charophytes actuelles et fossiles et phylogénie des genres actuels*. Imprimerie des Tilleuls, Millau, 1–237.

Soulié-Märsche, I. 1993. Diversity of aquatic environments in NE Africa as shown by fossil charophytes. *In:* Thorweihe, H. & Schandelmeier, R. (eds), *Geoscientific Research in Northeast Africa*. Taylor & Francis, Abingdon, 575–579.

Soulié-Märsche, I., Benammi, M. & Gemayel, P. 2002. Biogeography of living and fossil *Nitellopsis* (Charophyta) in relationship to new finds from Morocco. *Journal of Biogeography* **29**, 1703–1711.

Spezzaferri, S. 2004. Foraminiferal paleoecology and biostratigraphy of the Grund Beds (Molasse Basin–Lower Austria). *Geologica Carpathica* **55**, 155–164.

Spötl, C. & Vennemann, T.W. 2003. Continuous-flow isotope ratio mass spectrometric analysis of carbonate minerals. *Rapid Communications in Mass Spectrometry* **17**, 1004–1006.

Stancheva, M. 1966. Notes on the stratigraphy and the ostracode fauna from the Pliocene and post-Pliocene in the district of the Silistra. *Bulletin of Strashimir Dimitrov Institute of Geology, Ser. Paleontologie* **15**, 205–207.

Straub, E.W. 1952. Mikropaläontologische Untersuchungen im Tertiär zwischen Ehingen und Ulm an der Donau. *Geologisches Jahrbuch* **66**, 433–524.

Suzin, A.V. 1956. *Ostracoda from Tertiary Deposits of the North Caucasus*. Gostoptekhizdat, Moscow, 1–191 [In Russian].

Talbot, M.R. 1990. A review of the palaeohydrological interpretation of carbon and oxygen isotopic ratios in primary lacustrine carbonates. *Chemical Geology (Isotope Geoscience Section)* **80**, 261–279.

Taner, G. 1994. Paleotemperature findings from the Romanian and Bakunian stages of Çanakkale obtained from isotope analyses on mollusc shells. *Türkiye Jeoloji Kurultayi Bildiri Özleri* **47**, 12–13.

Taylor, S.R. & McLennan, S.M. 1985. *The Continental Crust: Its Composition and Evolution*. Blackwell, Oxford.

Tekin, E. 2001. Stratigraphy, geochemistry and depositional environment of the celestine-bearing gypsiferous formations of the Tertiary Ulaş-Sivas Basin, East-Central Anatolia (Turkey). *Turkish Journal of Earth Sciences* **10**, 35–49.

Tolosana-Delgado, R. 2012. Uses and misuses of compositional data in sedimentology. *Sedimentary Geology* **280**, 60–79.

Ünay, E., Bruijn, H. de & Sarac, G. 2003. A preliminary zonation of continental Neogene of Anatolia based on rodents. *Deinsea* **10**, 539–547.

Villwock, W. 1977. Das Genus *Aphanius* Nardo 1827. *Journal deutsche Killifisch Gemeinschaft* **9**, 165–185.

von Eynatten, H., Tolosana-Delgado, R. & Karius, V. 2012. Sediment generation in modern glacial settings: grain-size and source-rock control on sediment composition. *Sedimentary Geology* **280**, 80–92.

Walanus, A. & Nalepka, D. 1999. POLPAL. Program for counting pollen grains, diagrams plotting and numerical analysis. *Acta Palaeobotanica* Suppl. **2**, 659–661.

Wessels, W., Theocharopoulos, K.D., De Bruijn, H. & Ünay, E. 2001. Myocricetodontinae and Megacricetodontini (Rodentia) from the lower Miocene of NW Anatolia. *Lynx* **32**, 271–388.

Whatley, R.C. 1988. Population structure of ostracods: some general principles for the recognition of palaeoenvironments. *In:* De Deckker, P., Colin, J.P. & Peypouyet, J.P. (eds), *Ostracoda in the Earth Sciences*. Elsevier, Amsterdam, 245–256.

Wildekamp, R.H. 1993. *A World of Killies. Atlas of the Oviparous Cyprinodontiform Fishes of the World, Vol. 1*. American Killifish Association, Mishawaka IN, USA, 1–311.

Witt, W. 2010. Late Miocene non-marine ostracods from the Lake Küçükçekmece region, Thrace (Turkey). *Zitteliana A* **50**, 89–101.

Yildirim, C., Schildgen, T.F., Echtler, H., Melnick, D. & Strecker, M.R. 2011. Late Neogene orogenic uplift in the Central Pontides associated with the North Anatolian Fault - implications for the northern margin of the Central Anatolian Plateau, Turkey. *Tectonics* **30**, TC5005, DOI: 10.1029/2010TC002756.

Ziembińska-Tworzydło, M., Grabowska, I., Kohlman-Adamska, A., Skawińska, K., Stuchlik, L., Słodkowska, B., Ważyńska, H. & Sadowska A. 1994a. Taxonomical revision of selected pollen and spores taxa from Neogene deposits. *Acta Palaeobotanica* Suppl. **1**, 5–30.

Ziembińska-Tworzydło, M., Grabowska, I., Kohlman-Adamska, A., Skawińska, K., Stuchlik, L., Słodkowska, B., Ważyńska, H. & Sadowska A. 1994b. Checklist of selected genera and species of spores and pollen grains ordered in morphological system. *Acta Palaeobotanica*, Suppl. **1**, 31–56.

## Appendix

Taxonomy of Characeae from the Tuğlu section.

Order CHARALES Lindley 1836

Family Characeae L. Cl. Richard 1815

Genus *Nitellopsis* Hy 1889

***Nitellopsis* (*Tectochara*) *merianii*** (A. Braun ex Unger 1850) Grambast & Soulié-Märsche, 1972

1850 *Chara meriani* Al. Braun ex Unger, p. 50

1954 *Tectochara meriani* (Al. Braun ex Unger) Grambast & Grambast, p. 668

1972 *Nitellopsis* (*Tectochara*) *meriani* (Al. Braun ex Unger) Grambast & Soulié-Märsche, p. 11

1979 *Tectochara meriani* (Al. Braun ex Unger) Grambast 1954; Mädler & Staesche, p. 106

1997 *Nitellopsis* (*Tectochara*) *merianii merianii* (Al. Braun ex Unger) Grambast & Soulié-Märsche, 1972, Soulié-Märsche et al., p. 146–148, Figs 5, 6.

Description: Big, strongly calcified gyrogonites, size from 1000 to 1360 µm (average 1186 µm) in length and 760 to 1200 (average: 1012) µm in width. In lateral view, the outline of the gyrogonites varies from inversely pear-shaped to globular (average ISI: 118) with the main body prolonged by a rather short truncate column or conically pointed. Apex flattened in lateral view; apical nodes more or less protruding but spiral cells clearly narrowing at the apical periphery, apical nodes variable; 8–10, mostly 9 spiral turns visible in lateral view; spiral cells smooth; calcification varying from concave to flat or strongly convex.

Like other Miocene populations of *N. merianii*, the gyrogonites from the Tuğlu population show a majority of truncate basis with a broad basal funnel (60%). Another basal morphology (25%) comprises specimens with regularly diminished basis pointing downwards and surrounding the basal opening in a deep hollow.

The present gyrogonites are slightly bigger and larger than *Nitellopsis megarensis* Soulié-Märsche 1979 described from the Pliocene in Turkey (Rückert *et al*. 2002) and Late Pliocene in Kashmir (Bhatia *et al*. 1998).

Genus *Lychnothamnus* Rupr. v. Leonhardi emend A. Braun

***Lychnothamnus barbatus*** (Meyen) v. Leonhardi 1863

1989 **var. *antiquus*** nov. var. Soulié-Märsche 1989, p. 155, Pl. XXXVII, figs 1–9.

1979 = *Amblyochara anatolica* Mädler & Staesche 1979, p. 95, Pl. 4, figs 11–14.

Description: Gyrogonites of medium size, average of 850 µm high and 700 µm wide; shape mainly nearly rounded with constantly concave spiral cells separate by protruding simple sutures; rare specimens with double sutures; 9–10 turns visible in lateral view. Apex flattened; spiral cells not modified or slightly depressed at the apical zone. Sutures tending to become double around the small basal opening, where they form a star-like basal funnel.

Soulié-Märsche (1989) established the synonymy of genus *Amblyochara* Grambast with the extant genus *Lychnothamnus* and provided a reference diagram of the biometrical values of the gyrogonites of *L. barbatus*. The gyrogonites from the Tuğlu section display the same characters as the formerly described *Amblyochara anatolica* by Mädler and Staesche (1979), whose figures showed the same apical structure and the typical star-like basal funnel. Sample TU21 also showed very rare gyrogonites with double sutures similar to *Amblyochara bicarinata* (Mädler and Staesche 1979), suggesting that the latter may be probably only a variant of *L. barbatus antiquus*.

*A. anatolica* was recorded from Oligocene to basal Quaternary (Calabrian) with Sekköy as the type locality.

Genus *Chara* Linnaeus

***Chara* cf. *molassica*** Straub 1952

1979 *Charites molassica* (Straub) Horn af Rantzien 1959, Mädler & Staesche, p. 85, Pl. 1 Fig. 1–5.

1989 *Chara molassica* Straub, Soulié-Märsche 1989, p. 146.

Sample 21 of the Tuğlu section displayed only 3 gyrogonites of genus *Chara*. These medium-sized specimens (c. 600 µm high and 420 µm wide) display the typical ovoid *Chara* morphology and are tentatively attributed to *Chara molassica*.

The gyrogonites of *Chara molassica* consist of very simple ovoid specimens very frequent all over the European Miocene. They must be considered at least the ancestor of, if even not identical to, living *Chara vulgaris* L. Already Mädler and Staesche (1979) have noted the close similarity of *Chara molassica* with the gyrogonites of the living *Chara vulgaris* (cited as *Chara foetida*).


**Plate 1.** SEM photographs of the foraminifera and otoliths from the Tuğlu section. (a) *Quinqueloculina pauperata* Orbigny. (b) *Quinqueloculina* cf. *akneriana* Orbigny. (c–d) *Aphanius* otolith. (e–f) *Miliammina velatina* Venglinski. (g–h) *Varidentella reussi* (Bogdanowicz). (i) *Articulina* aff. *tamani* Bogdanowicz. (j–k) *Trisegmentina compressa* Wiessner (all from sample TU4).

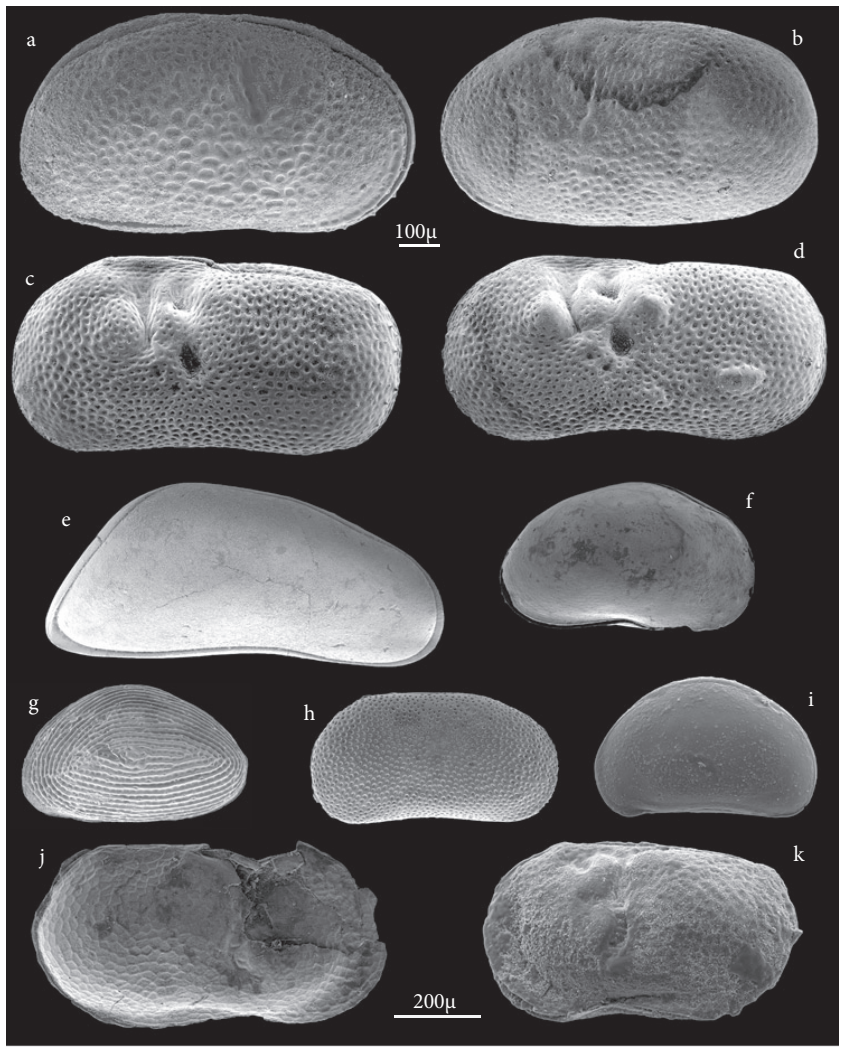


**Plate 2.** SEM photographs of ostracods from the Tuğlu section. All specimens are figured in external lateral view. (a–b) *Cyprideis sublittoralis adentata*: (a) carapace RV TU6, (b) LV (TU4). (c–d) *Ilyocypris* cf. *decipiens*: (c) LV (TU13), (d) LV, tuberculate form (TU13). (e) *Candona* (*Caspiocypris*) *postsarmatica*, carapace RV (TU9). (f) *Heterocypris* cf. *gregaria*, carapace LV (TU37). (g) *Zonocypris membranae quadricella*, LV (TU24). (h) *Marchiella* cf. *hartwigi*, RV (TU18). (i) *Cypria* sp., RV (TU34). (j) *Leucocythere camenice*, RV (TU34). (k) *Limnocytherina* sp., LV (TU17). a, b, c, d, e, f, g, h, i: scale bar = 100 µm. j, k: scale bar = 200 µm.

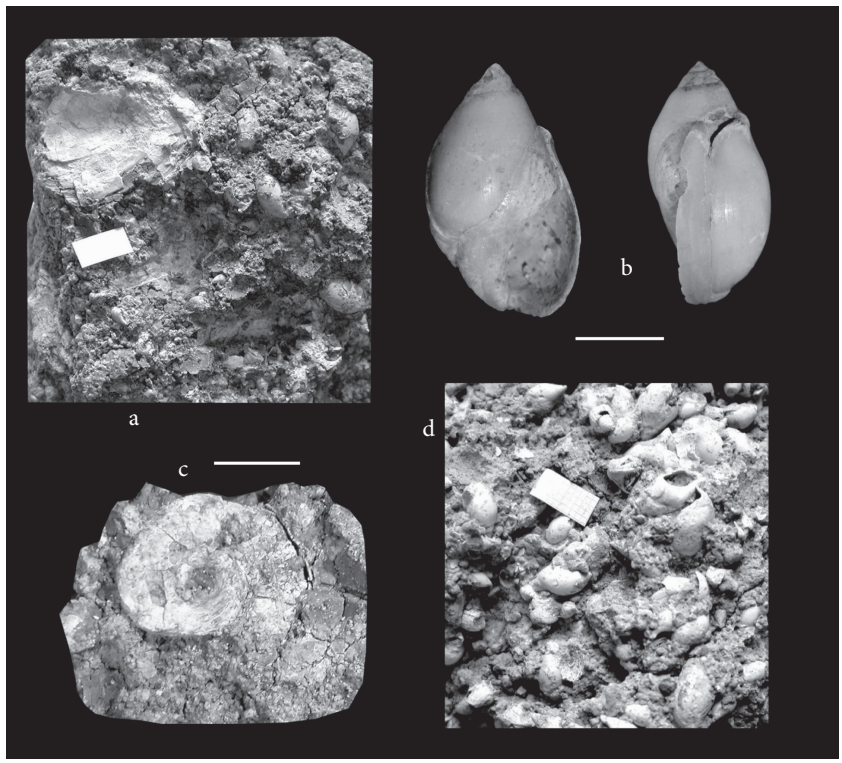


**Plate 3.** SEM photographs of molluscs from the Tuğlu section. (a, d) Mollusc assemblage from sample TU42, *Melanopsis obesa* Brusina and *Potomida* sp. are visible. Measure = 1 cm. (b) *M. obesa*, scale bar = 5 mm. (c) *Planorbarius* sp., sample TU23, scale bar = 7 mm.

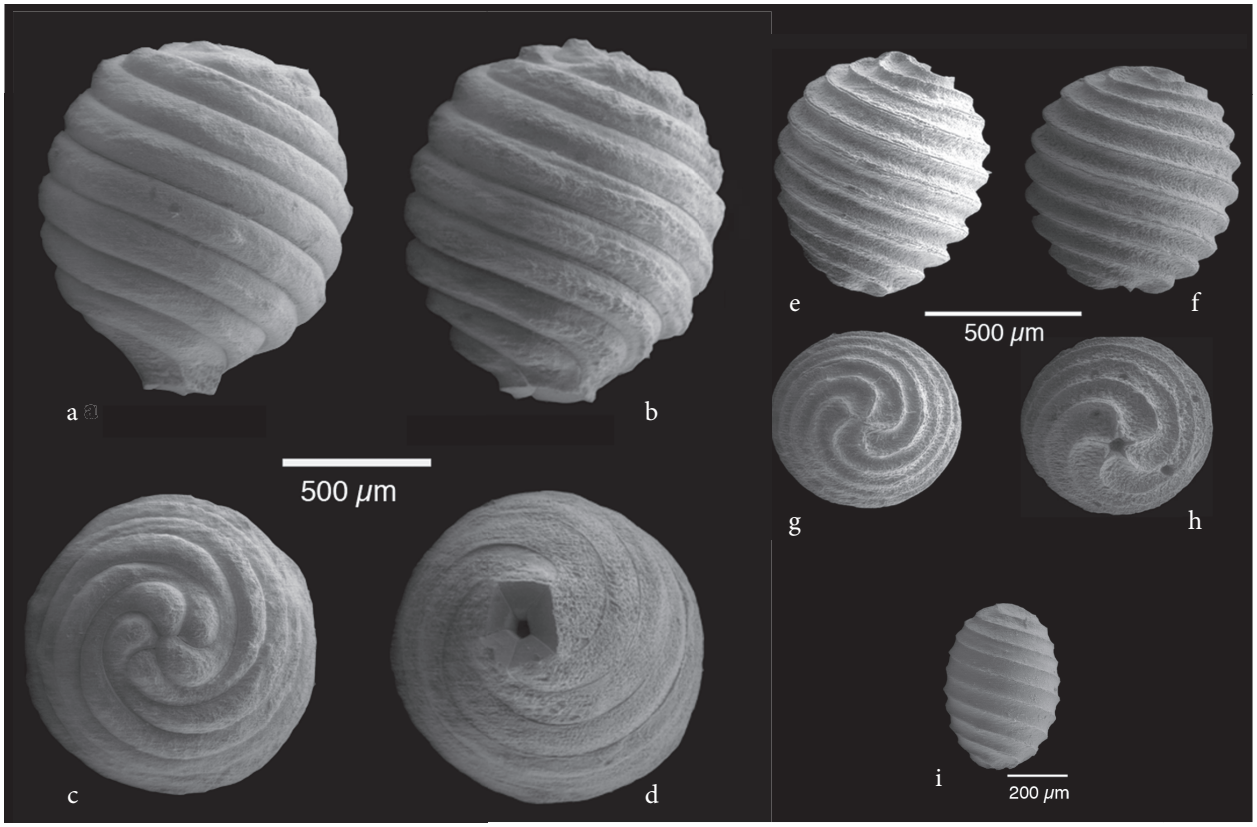


**Plate 4.** SEM photographs of charophyte gyrogonites from the Tuğlu section. (a–d) *Nitellopsis merianii*: (a–b) lateral view with truncate basis, (c) apical nodes, (d) basal opening and basal funnel. (e–h) *Lychnothamnus barbatus* var. *antiquus*: (e–f) lateral view, (g) apical view, (h) star-like basal opening. (i) *Chara* cf. *molassica*, lateral view (all from sample TU21).